CR-152,305

BK028-1001

ADVANCED THERMAL CONTROL FLIGHT EXPERIMENT (ATFE) -- FINAL REPORT

(NASA-CR-152305) ADVANCED THERMAL CONTROL FLIGHT EXPERIMENT (ATFE) Final Report (B & K Engineering, Inc., Towson, Md.) 61 p HC A04/MF A01 CSCL 20D

N79-29474

Unclas

G3/34 34425

July 30, 1979

Prepared for

NASA Ames Research Center

Under

Purchase Order No. A-33703-B (DG)

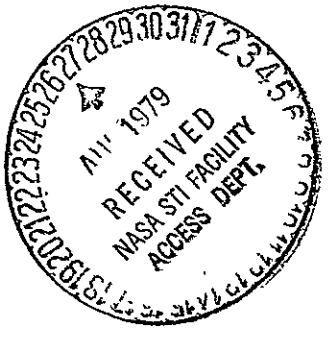

By

B & K ENGINEERING, INC.
Suite 825, One Investment Place
Towson, Maryland 21204

SUMMARY

The Advanced Thermal Control Flight Experiment (ATFE) contains a thermal diode, a phase change material (PCM) package and a feedback controlled heat pipe (FCHP) which are integrated with a solar absorber and a space radiator into a thermal control system. For the past five years this system has been in a geosynchronous orbit aboard the Applications Technology Satellite-6 (ATS-6). Its outboard surface, which views deep space, has received a daily solar exposure similar to that experienced by a fixed point on the Earth's surface. This solar input has continuously exercised the ATFE components for more than five years with the End of Mission (EOM) date being obtained July 3, 1979.

The thermal diode performed effectively as an OFF/ON thermal switch. It carried an average of 20 W in the forward mode and demonstrated an OFF conductance of less than 0.03 W/°C. It has exhibited some apparent non-condensible gas generation which subsided after the first two and one half years. This increased the forward mode temperature drop and led to an initial decrease in the reverse mode conductance.

The octadecane PCM package provided temperature stability in accordance with its design. Its melting and freezing points remained stable at 27.9 and 27.4°C, respectively, through five years of daily cycles. Its thermal conductance was unaffected by the 0-g environment and any subcooling effects were negligible. The 26 W-hr. of latent heat energy that it supplied allowed the simulated equipment package to stabilize at the freezing point of 6.4 hours during the shadow period in the normal operational mode.

The FCHP also demonstrated its effectiveness as a thermal control component. It daily transported a forward mode heat load of approximately 20 W and carried up to 30 W in auxiliary mode tests. It operated as an ON/OFF thermal switch by isolating the PCM from the radiator during the shadow period. Its OFF conductance was also less than 0.03 W/°C.

The FCHP was unable to control at the 29°C design set point because the gas reservoir was running hotter than the nominal design conditions. It was determined that the higher reservoir temperatures were caused by degradation of the second surface mirrors (Optical Solar Reflectors-OSR) which cover the reservoir's radiator. The effective absorptivity of the OSRs has steadily increased throughout the mission. Their nominal value was taken as 0.10, whereas they demonstrated an absorptivity of 0.19 initially in space which increased to approximately 0.47 at the end of the mission. The FCHP's temperature control capability was demonstrated, however, by tests in which a higher control point (46°C) was used to overcome the limitation imposed by the hot reservoir. The feedback system in this test provided control to within ± 2°C while the sink temperatures varied 82°C.

In conclusion, the ATFE has met all design objectives throughout more than five years of flight operation. It can be concluded that feedback controlled heat pipes, thermal diode heat pipes, and phase change materials are flight worthy. Their designs are readily available and their behavior is well understood. Finally, their long term performance is well established and on the basis of the ATFE experience, highly reliable.

1.0 INTRODUCTION

This report presents a comprehensive description of the design and performance of the Advanced Thermal Control Flight Experiment (ATFE). This experiment was launched aboard the Applications Technology Satellite-6 (ATS-6) on May 30, 1974. Flight data was monitored during the following five years. End of life data was obtained July 3 and 4, 1979. The ATFE was designed to demonstrate for the first time in a space environment, the performance of a thermal diode heat pipe, a phase change material (PCM) and a feedback-controlled variable conductance heat pipe (FCHP). The steady state and transient ground and flight performance of these individual components and the entire experiment is analyzed.

2.0 EXPERIMENT OBJECTIVES

The ATFE design permits evaluation of the thermal diode, PCM and FCHP on an individual basis and as an integrated temperature control system. In addition to developing flight qualified hardware for future thermal control applications, specific ATFE performance objectives were as follows:

1) Thermal Diode: Demonstrate forward and reverse mode diode operation in a 0-g environment.

2) Phase Change Material: Demonstrate the temperature stability derived from the melting and freezing of a PCM: determine the stability of the melting and freezing points in the 0-g environment; and evaluate the effect of the 0-g environment on the thermal conductance of the PCM package.

3) Feedback Controlled Variable Conductance Heat Pipe: Demonstrate the ability of the FCHP to provide temperature stability with variations in heat load and effective sink temperature and evaluate its performance as an ON/OFF thermal switch.

3.0 SYSTEM DESCRIPTION

A schematic of the ATFE is presented in Fig. 3-1. The ATFE consists of a solar absorber, a thermal diode, a simulated equipment package that contains phase change material (PCM), a feedback controlled variable conductance heat pipe (FCHP), and a space radiator. Supporting hardware not shown in Fig. 3-1 are a solid state electronics module, temperature sensors, foil heaters, multilayer thermal insulation blankets, and a support structure. The electronics module contains the controller for the feedback controlled heat pipe, signal conditioning circuitry, and command relays. The functional relationship of the ATFE components is represented in Fig. 3-2.

The ATFE is mounted in the east wall of the earth-viewing module of the ATS, with only the outboard surfaces of the solar absorber and radiator exposed to the external environment. Solar input is used as the primary heat source of the experiment. Because of the geosynchronous orbit and three-axis stabilization, the solar flux incident upon the east wall and the ATFE rises and sets with an approximately sinusoidal variation over a 12 hour period, followed by 12 hours of shadow (Fig. 3-3). The solar cycle is essentially the same as that experienced by a fixed point on the earth's surface.

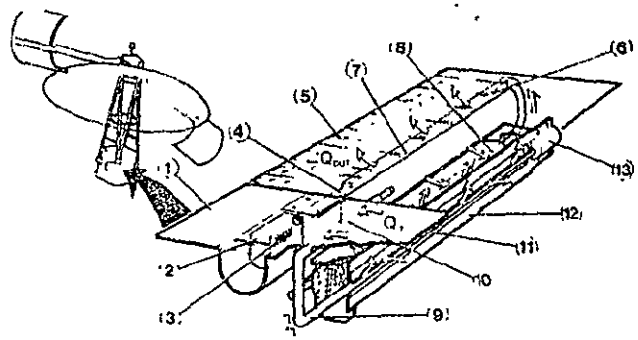

1 SOLAR ABSORBER
2 GAS RESERVOIR
3 CONTROL HEATER
4 GAS/VAPOR INTERFACE
5 RADIATOR
6 FEEDBACK CONTROLLED HEAT PIPE (FCHP)
7 FCHP CONDENSER SECTION
8 FCHP EVAPORATOR SECTION
9 THERMAL DIODE HEAT PIPE
10 DIODE EVAPORATOR SECTION
11 DIODE CONDENSER SECTION
12 PHASE CHANGE MATERIAL (PCM) BOX
13 LIQUID RESERVOIR

Fig. 3-1. Advanced thermal control flight experiment (ATFE)

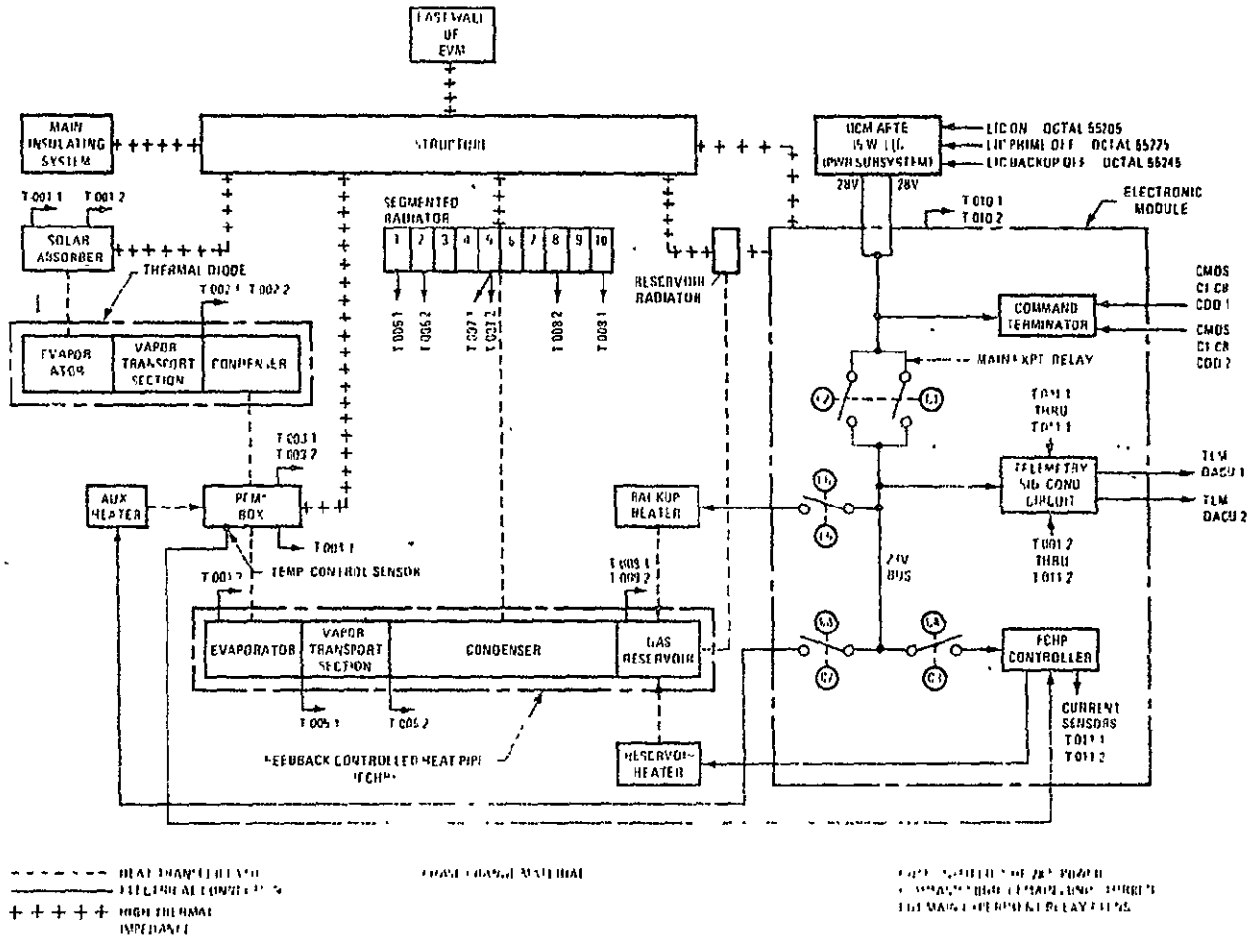

Fig. 3-2. Functional diagram

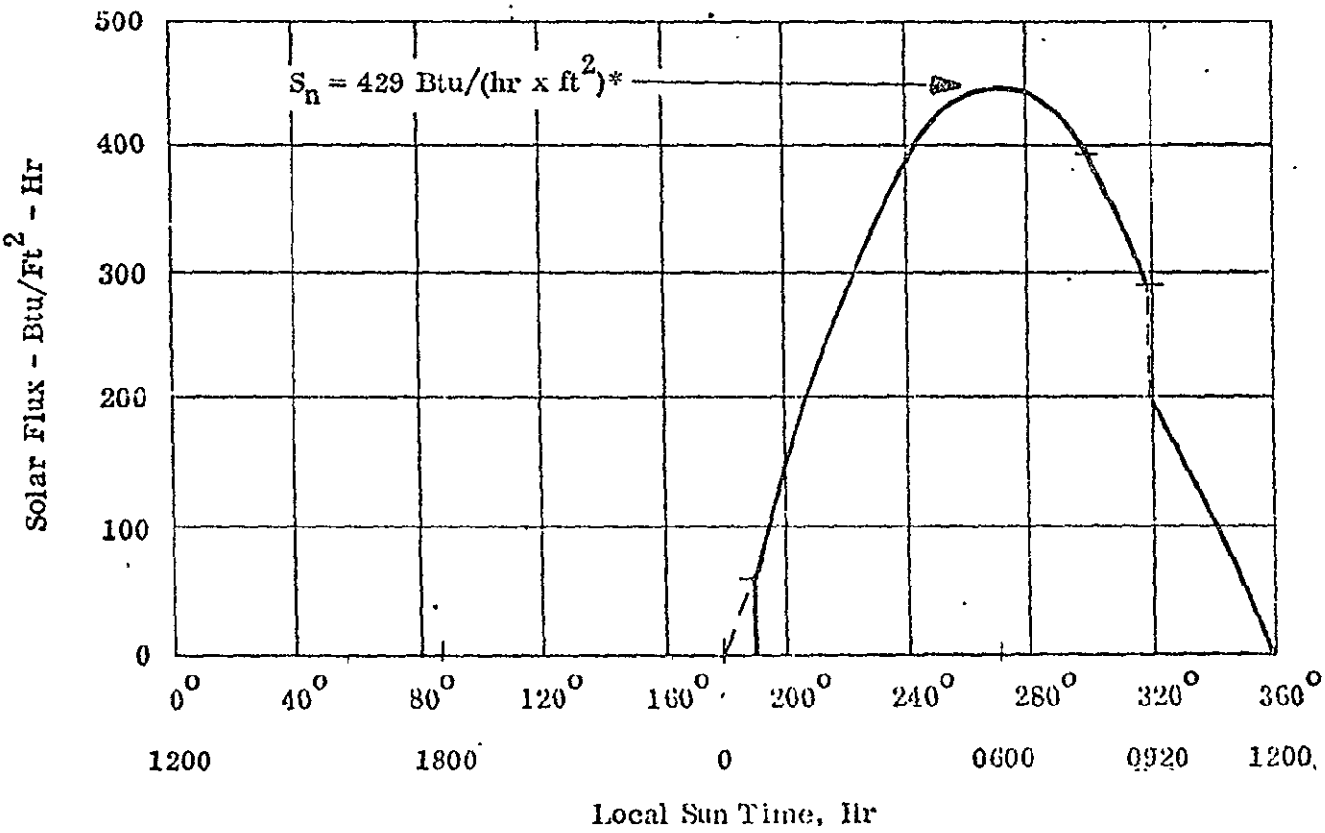

*Not plotted to scale

Fig. 3-3. Typical daily solar cycle for ATFE

During the period of solar input, energy collected by the absorber is transported by the diode heat pipe to the PCM box. This energy is equivalent to power dissipation during an electrical duty cycle, with the PCM package serving as a simulated temperature-controlled equipment shelf. Initially, the energy melts the PCM, which is octadecane with a melting point of 28°C. When all of the PCM has melted, the energy from the absorber passes through the equipment shelf to the FCHP, which transports it to the space radiator. During this part of the cycle, temperature control of the diode/PCM box interface is provided by the FCHP. A sensor at this interface enables the FCHP to regulate the heat rejection to space and thereby accommodate variations in both the thermal load and the thermal boundary conditions at the radiator. The feedback system was designed to control the diode side of the PCM box at 29 ± 3°C.

As the shadow period is approached, the diode and FCHP decrease their conductance to minimize the heat loss from the PCM box to space. This occurs in the following manner. As the heat input to the system diminishes, the absorber radiator and PCM box begin to cool. When the absorber temperature drops below the temperature at the diode side of the PCM, passive shut-down of the diode occurs, which thermally decouples the cold absorber from the PCM box. Similarly, under normal FCHP operation, when the PCM temperature drops below 29°C, the FCHP shuts down and decouples the box from the cold radiator. With no thermal throughput, the PCM continues to cool to 28°C and then begins to freeze.

Thermal energy released by the freezing of the octadecane is used to compensate for the heat loss during transient shutdown of the diode and the FCHP, and to provide for temperature stability over part of the 12 hour shadow period. When all the octadecane has frozen, the temperature of the equipment shelf decreases at a rate consistent with the thermal capacitance of the PCM box and its parasitic heat leaks. There is 0.363 kg of octadecane which provides temperature stability for about five hours of shadow, after which the PCM box cools to approximately 0°C. The temperature of the PCM was allowed to decrease to 0°C in order to evaluate the effect of subcooling on the stability of the melting point of the octadecane.

The ATFE has five operational modes in addition to the normal mode just described. Each of these modes is defined in Table 3-1. Several modes permit continued operation in the event that the thermal diode or FCHP controller fails. The Passive and Passive-Auxiliary modes are used to obtain performance data with the FCHP operating as a conventional gas-controlled heat pipe. Finally, the Auxiliary and Back-Up Heaters can be utilized to demonstrate extended performance capability by the FCHP at temperatures different from the controller set point (29°C).

TABLE 3-1. ATFE OPERATIONAL MODES

Mode	Description	Command Status
Normal	Normal operation of system: Controller provides automatic regulation by FCHP.	ATFE Experiment Turn ON ATFE FCHP Controller ON
Auxiliary	Auxiliary Heater ON, to provide additional exercise of FCHP or redundancy if thermal diode should fail.	ATFE Experiment Turn ON ATFE FCHP Controller ON ATFE PCM Box Auxiliary Heater ON*
Passive	FCHP Controller turned OFF: FCHP acts as a passive variable conductance heat pipe.	ATFE Experiment Turn ON
Passive-Auxiliary	FCHP Controller OFF and Auxiliary heater ON as in Auxiliary Mode, to evaluate system with passive control.	ATFE Experiment Turn ON ATFE PCM Box Auxiliary Heater ON
Back-Up	Manual control of the back-up reservoir heater, to provide redundancy in the event the FCHP Controller should fail, or operation at an alternate set point.	ATFE Experiment Turn ON ATFE FCHP Back-Up Reservoir Heater ON/OFF**
Back-Up/ Auxiliary	This mode is redundant to the Auxiliary Mode, with manual control of the Back-Up Heater. It can also be used to demonstrate additional FCHP performance at temperatures different from the FCHP controller's set point.	ATFE Experiment Turn ON ATFE FCHP Back-Up Reservoir Heater ON/OFF** ATFE PCM Box Auxiliary Heater ON

*The auxiliary heater is attached to the diode side of the PCM box and has a 20-W electrical output.

**The back-up heater is attached to the FCHP's reservoir and is redundant to the reservoir heater regulated automatically by the controller. It has a 2.8-W output and is turned ON or OFF by command, as needed, to maintain control at the desired set point.

4.0 COMPONENT DESIGN

4.1 Absorber

The absorber consists of a 0.040 in. (0.102 cm) thick aluminum substrate coated with Chemglaze Z306 (α/E = 0.96/0.86) and has a 6 x 12 in. (15.24 x 30.48 cm) platform. A black point was chosen to maximize the solar absorption while minimizing the absorber's equilibrium temperature during peak solar conditions. Also, the high emittance results in a lower absorber temperature during the shadow, thereby providing a better test of diode performance. If the FCHP should fail to transport the heat input, the absorber, diode, and PCM box would approach the equilibrium's temperature of the absorber. The maximum allowable temperature in this failure mode was set at 127°C to guarantee a reasonable margin of safety for these components. Coatings with lower emissivities would have resulted in a more efficient absorber system, but their equilibrium temperatures would have been unacceptable. Six 1 in. (2.54 cm) square optical solar reflectors (OSR, α/E = 0.10/0.82) are attached at one edge of the absorber to further guarantee the 127°C maximum temperature.

As indicated in Fig. 3-1, the absorber has a 2 in. (5.08 cm) diameter "well" located near its center. This well runs the length of the absorber and accommodates the reservoir of the FCHP. Both sides of the well are insulated with multilayered insulation to minimize thermal interaction with the reservoir and to provide an essentially adiabatic surface. Adjacent to the well is a 5 in. (12.70 cm) long aluminum saddle that was welded as an integral part of the absorber panel. The evaporator section of the diode is soldered to this saddle.

The total absorbing area is 60 in.^{2} (387 cm^2), and the efficiency is approximately 45%. This results in a thermal throughput of approximately 20 W for a maximum solar constant of 1418 W/m^2. The length of the absorber was sized to maximize the net thermal input, consistent with the experiment envelope and radiator heat rejection requirements.

4.2 Thermal Diode Heat Pipe

The development of thermal diode heat pipe technology is presented in Ref. 1.* Various methods exist for accomplishing diode heat pipe operation. These include gas-blockage, liquid-blockage, liquid-trap, and mechanical techniques. The excess liquid-blockage technique was selected for the ATFE because it requires a significantly smaller reservoir volume than gas-blockage and liquid-trap designs and heat losses associated with transient shutdown are generally less, at least for comparable passive systems.

The liquid-blockage technique is based on the principle that excess liquid will accumulate as a slug in the cold section of the pipe. This slug inhibits vapor flow, thereby preventing "heat-piping" action in the blocked section and, except for relatively small conduction losses, effectively limits the heat transfer. A reservoir is located at the condenser end to accommodate excess liquid during the normal, or forward, heat-pipe mode.

*The diode was provided as Government Furnished Equipment from Grumman Aerospace Corporation to Dynatherm Corporation for utilization in the ATFE.

In the ATFE, as the shadow period is approached, the absorber temperature drops below the temperature of the PCM box. When this happens, the liquid and vapor flows in the diode are reversed; the normal condenser becomes an evaporator and the normal evaporator a condenser. The excess liquid in the reservoir is vaporized by heat losses from the PCM box and flows to the reverse mode condenser (absorber end). There it condenses, fills the vapor space, and effectively blocks further heat flow.

The detailed design of the ATFE diode has been previously reported (Ref. 2) and, therefore, only the major points will be discussed. The basic configuration is shown in Fig. 4-1 and summarized in Table 4-1. During shutdown, the vapor space in the evaporator, low "k", and transition sections must be blocked, hence the smaller tube I.D. and vapor-space thickness in these sections. The larger I.D. and corresponding vapor-space thickness in the condenser section is used to reduce the vapor pressure drop in the forward mode. To minimize conduction losses, the low "k" section has a wall thickness of only 0.010 in. (0.0254 cm). It is reinforced with fiberglass to increase its burst pressure and protect it during handling.

The tunnel wick fabricated from 100-mesh screen is used as the primary capillary structure. The artery is centrally located and supported by a three-legged screen retainer-web assembly. This retainer also serves as a communication link between the artery and the screw thread grooves (80 in. or 31.5 cm) which provide circumferential distribution of the liquid around the tube. The spiral

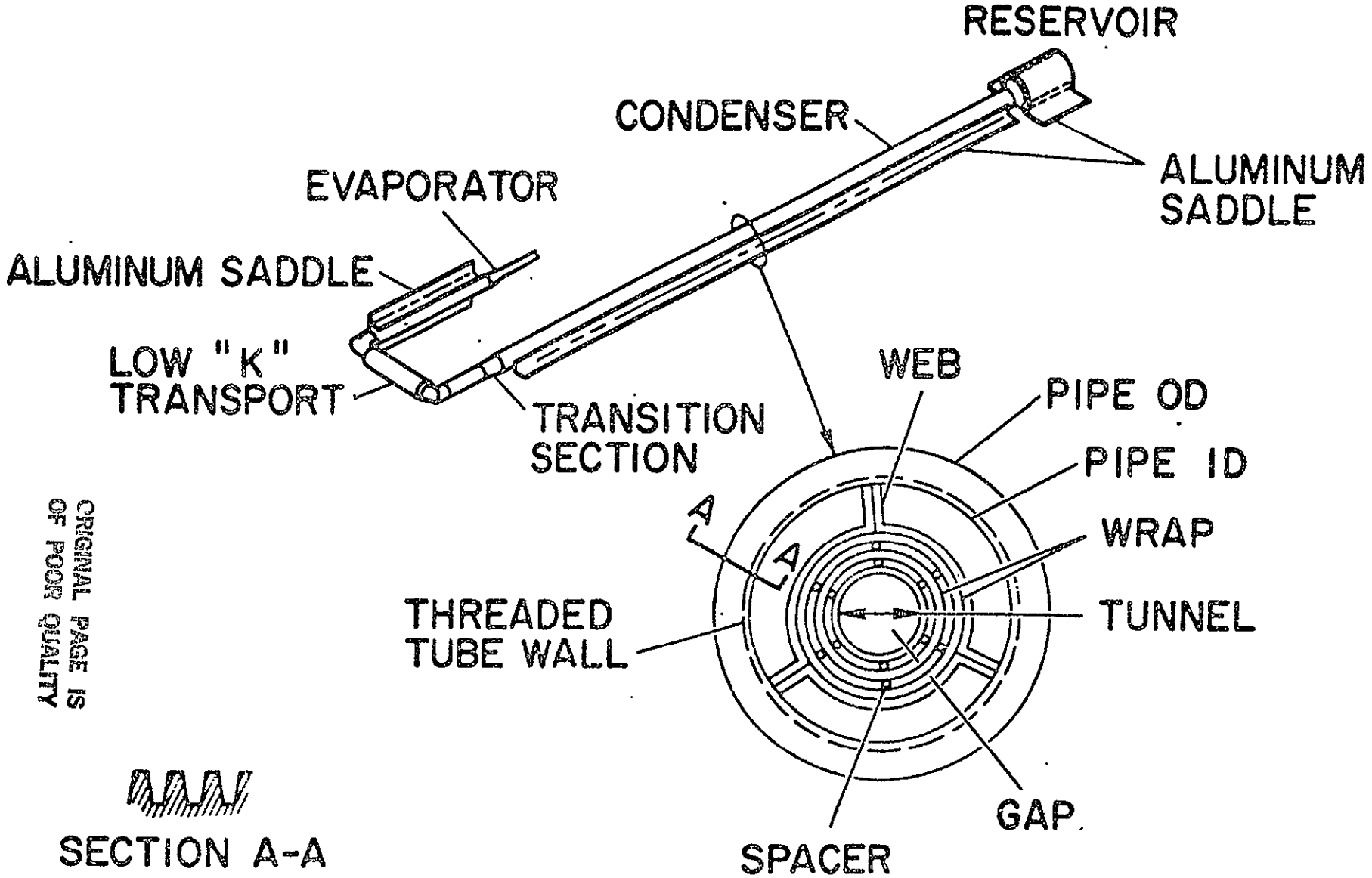

Fig. 4-1. Diode heat pipe

TABLE 4-1. ATFE DIODE HEAT PIPE SUMMARY

Envelope material -- 304 stainless steel
Wick - 100-mesh stainless steel tunnel spiral artery
Working fluid ammonia, 17.5 gm
Reservoir volume = 6.05 cm^3
Weight (diode only) = 286 gm

Section	Length, in. (cm)	O.D., in. (cm)	I.D., in. (cm)	Vapor space thickness, in. (cm)
Evaporator	4.90 (12.45)	0.377 (0.96)	0.309 (0 78)	0.025 (0 064)
Low "K"	1 88 (4 78)	0.329[a] (0.84)	0.309 (0 78)	0.025 (0 064)
Transition	1 42 (3 61)	0.375 (0.95)	0.309 (0 78)	0.025 (0.064)
Condenser	18 08 (45 92)	0.452 (1.15)	0.411 (1.04)	0.074 (0.190)
Reservoir	1 44 (3 66)	1.000 (2.54)	0.884 (2.25)	- -

[a]Tube without fiberglass reinforcement.

TABLE 4-2. ATFE FCHP SUMMARY

Envelope material -- 304 stainless steel
Wick -- 325/20 mesh stainless steel screen composite (0 12 in thick)
Working fluid methanol, 28 gm
Control gas helium, 2 08×10^{-3} gm
Reservoir volume '8 cm^3
Reservoir volume/condenser and transport section vapor space 5 0 cm^3
Weight (including saddles) -- 489 gm

Section	Length, in. (cm)	O.D., in. (cm)	I.D., in. (cm)
Evaporator	18.9 (48.00)	0.438 (1.113)	0.382 (0.970)
Transport	4.5 (11.43)	0.438 (1.113)	0.382 (0.970)
Condenser	15.7 (39.88)	0 375 (0 953)	0.319 (0 810)
Feed tube	2.5 (6.35)	0.375 (0.953)	0 345 (0.876)
Reservoir	2.9 (7.37)	N/A N/A	N/A N/A

TABLE 4-3. ATFE COMMAND ASSIGNMENTS[a]

Command title	Command function
Experiment ON	Applies 28 vdc from the spacecraft to the experiment bus
Experiment OFF	
Controller ON	Applies 28 vdc from the experiment bus to the controller
Controller OFF	
Backup heater ON	Applies 28 vdc from the experiment bus to the backup heater
Backup heater OFF	
Auxiliary heater ON	Applies 28 vdc from the experiment bus to the auxiliary heater
Auxiliary heater OFF	

[a]Each of the OFF command functions removes the 28 vdc applied by the corresponding ON command.

artery design permits relatively high heat-transport capability in the normal mode with a small hydraulic diameter for the vapor flow, which is needed to support the liquid across the internal tube diameter in the blocked portion during shutdown in the 1-g environment. The smaller diameter also reduces the amount of excess liquid required, thereby decreasing the transient energy losses during shutdown and also the reservoir size.

The diode reservoir consists of 86 independent 0.063 in. (0.160 cm) diameter channels drilled in an aluminum cylinder 1.44 in. (3.66 cm) long. Aluminum was used to increase the heat-transfer rates during the direct-to-reverse mode transient, thereby reducing the shutdown time and the transient losses. The aluminum is press-fit into a stainless-steel shell that is welded to the condenser tube. The arterial wick extends through the heat-pipe tube but does not communicate with the liquid reservoir. Aluminum saddles are soldered to the reservoir and condenser to provide for attachment to and heat transfer to the PCM box.

4.3 Phase-Change Material (PCM) Box

Phase-change materials, also referred to as fusible materials, provide temperature stability by absorbing or rejecting heat nearly isothermally as they melt or freeze. In the ATFE, the latent heat of fusion released by freezing the PCM is used to compensate for both transient and steady-state parasitic losses from the PCM box. The transient losses are experienced during shutdown of the diode and

FCHP components as the shadow period is approached. The parasitic losses occur during the shadow and are associated with (1) conduction leaks through the diode, FCHP, and structure and (2) radiative coupling of the PCM box through its insulation to the cold absorber and radiator sysems.

Fig. 4-2 is a sketch showing the details of the PCM box. In addition to housing the PCM, the diode side of the box is used as a simulated equipment platform whose temperature is regulated by the FCHP during periods of heat input. The PCM box is a welded aluminum assembly with 0.040 in. (0.102 cm) thick walls. The box was designed to have a 10 W/°C conductance from diode to FCHP side.

Two identical compartments in the box contain the PCM, which is distributed in a partially expanded aluminum honeycomb core. Hysol adhesive is used to bond the honeycomb within the box.

The honeycomb core is used to increase the thermal diffusivity of the PCM system and was designed in accordance with the procedure recommended in Ref. 3. The individual compartments reduced the effective conduction length through the PCM/honeycomb core, thereby decreasing the amount of honeycomb required for optimum performance. In this system, the honeycomb cells have been oriented so that the primary conduction path is from the center shunt and side member to the center of the compartment. The side members and the center shunt are 0.040 in. (0.102 cm) and 0.031 in. (0.078 cm) thick, respectively. The different thicknesses result in equal conductance paths through and around the box.

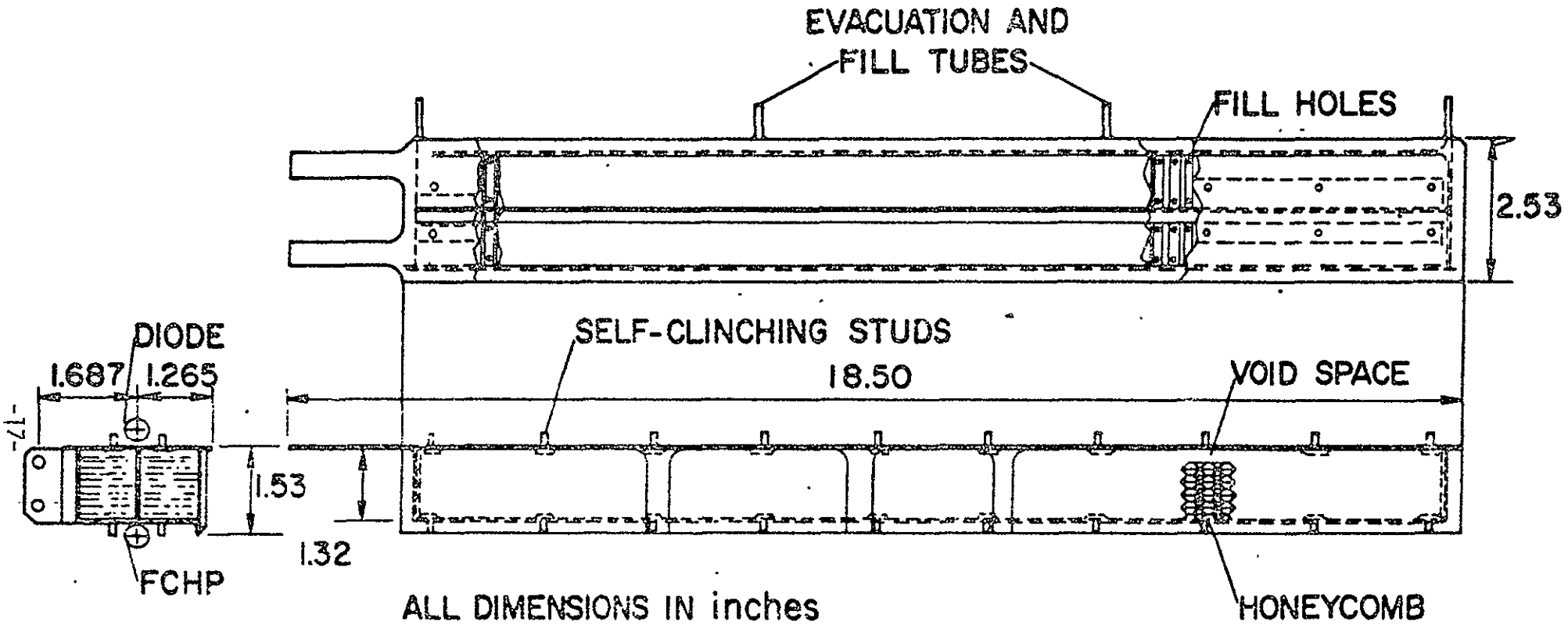

Fig. 4-2. PCM box

The PCM box contains 384 gm of octadecane, which is equivalent to 26 W-hr. of latent heat energy. Octadecane was chosen because its melting temperature (28°C) was within the desired operating range and because it is an n-paraffin. These paraffins have a number of desirable features, including high heat of fusion and melting point stability (Ref. 4). Practical grade octadecane was used instead of a purer grade because the impurities provide more nucleation sites that facilitate solidification.

A void space of approximately 15% of the total internal volume is located above the honeycomb core at the diode side of the box to accommodate expansion of the octadecane up to a temperature well above the FCHP failure-mode temperature of 127°C. Two 0.0625 in. (0.159 cm) holes are drilled through each individual cell of the honeycomb to permit charging with the PCM and also to allow for expansion of the melted liquid into the void space. The void is purposely located near the heat input side of the box to allow the melting liquid to flow uninhibited toward a void. This prevents any localized excessive pressure buildup during liquefaction. For this same reason, the holes are located near the edges of the cells where the heat flows into the honeycomb from the conduction members.

The smallest characteristic dimension of the void is substantially larger than the smallest characteristic dimension of the honeycomb cell. As a result, in 0-g, because of capillary action the liquid will preferentially-fill the honeycomb. If the void had not been designed in this manner, a vapor space could have formed around the periphery of the individual compartments. This would result in poor conduction to the PCM and possibly only partial melting or freezing.

Two 0.125 in. (0.3175 cm) charging tubes are welded to one side of the box. The box is first evacuated and then charged with the PCM at 125°C. A number of 0.125 in. (0.3175 cm) holes are located in the center member to allow charging of the individual compartments in a single operation. Self-clinching studs are inserted into the diode and FCHP faces of the PCM box to provide for mechanical attachment of these components. The PCM box is bolted to the support structure through flanges located at the end plates.

4.4 Feedback-Controlled Heat Pipe (FCHP)

Both active and passive methods exist for obtaining feedback control with variable conductance heat pipes (Ref. 5, 6, 7). The development of an active system, however, was pursued for the ATFE because of its greater temperature control capability, simpler mechanical design, and fewer potential startup problems. The active system is shown schematically in Fig. 4-3. It is basically a gas-controlled wicked reservoir heat pipe (Ref. 8) that utilizes an electronic controller and a reservoir heater to adjust its thermal conductance. An increase in heat-source temperature caused by an increase in heat load and/or sink condition results in an error signal to the controller, causing it to reduce the power to the reservoir heater. The corresponding decrease in reservoir temperature and therefore in the vapor pressure of the working fluid in the reservoir results in an increase in the effective storage volume, thereby allowing more non-condensible gas to enter. This causes the gas-vapor interface to move

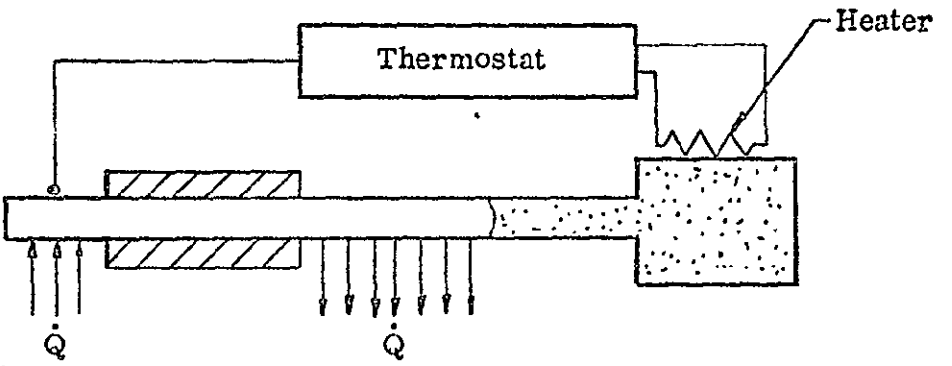

Fig. 4-3. Feedback control

toward the reservoir, thus increasing the condenser conductance and ultimately reducing the source temperature. The continual adjustment of the conductance by regulating from the controller can provide essentially absolute temperature control under broad variations in heat load and sink conditions.

The basic ATFE FCHP configuration is shown in Fig. 4-4 and summarized in Table 4-2. Methanol was selected for the working fluid because it provides adequate self-priming and transport capability and its vapor pressure is substantially lower than that of ammonia. Consequently, a significantly lighter reservoir can be used for containment, resulting in more rapid response of the FCHP system to perturbations of the source temperature (Ref. 9).

A composite slab wick was fabricated by wrapping 325-mesh screen around alternate layers of 325 and 20 mesh. It is centrally located in the heat pipe tube. The coarse screen permits high permeability within the limits of self-priming requirements, whereas the fine screen is used to establish a high capillary pumping head. Screw thread grooves (36 in. or 14.17 cm) provide circumferential distribution of the liquid.

The evaporator and transport sections of the FCHP have a 0.382 in. I.D. and the condenser section has a 0.319 in. I.D. The larger I.D. is required to reduce viscous vapor losses and provide adequate transport capability, whereas the smaller condenser reduces the reservoir storage requirements. The feeder tube that extends from the condenser to the reservoir was reamed to a 0.015 in (0.0381 cm) wall thickness to minimize conduction losses.

The reservoir's cross section (Fig. 4-4) was designed to minimize the self-priming requirement and to keep the reservoir radiator flush with the absorber to minimize solar input to the reservoir during maximum solar conditions, thereby allowing the reservoir to cool more efficiently. The reservoir has a 7.0 $in.^2$ (45.16 cm^2) OSR-covered radiating surface. The ratio of reservoir volume to condenser volume and the amount of non-condensible gas was chosen to provide temperature control of the PCM box at 28°C with the reservoir temperature varying from -8° to +8°C at maximum and minimum conditions, respectively.

A solid-state on/off electronic controller is used to provide regulation of the foil heater attached to the reservoir. A thermistor is used as the temperature sensor.

Aluminum saddles are soldered to the evaporator and condenser sections to provide attachment to the PCM box and to the radiator panels. The condenser saddles are segmented to minimize conduction losses and establish a sharp gas-vapor interface.

4.5 Radiator

The radiator consists of 10 separate aluminum panels 0.040 in. (0.102 cm) thick and 12.0 in. (30.48 cm) wide. Since the radiator must reject its maximum energy during full sun, the panels are covered with OSRs whose specified optical properties are α/ε = 0.06/0.82. However, an absorptivity of 0.10 has been used as a design

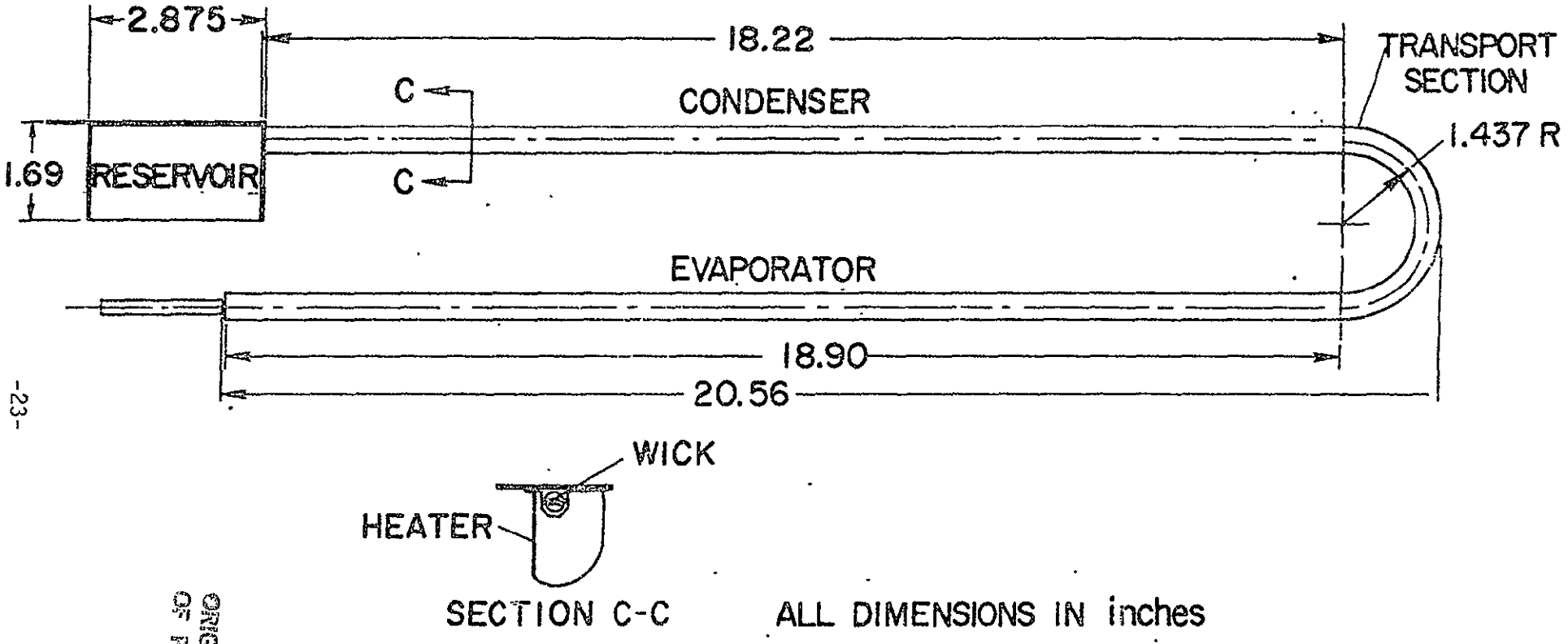

Fig. 4-4. Feedback control heat pipe

value for all OSR surfaces to allow for spaces between the OSR's (i.e., packing factor), contamination, and potential infrared input from the spacecraft. Self-clinching studs are pressed into the panels to allow attachment to the FCHP condenser saddles and the ATFE support frame. Once installed, the radiator has a 17.75 x 12.0 in. (45.09 x 30.48 cm) platform.

4.6 Electronics Module

The electronics module contains the controller, command circuitry, and signal conditioning for the ATFE telemetry, as shown in Fig. 3-2. Its electrical interface with the spacecraft is represented in Fig. 4-5.

4.6.1 Controller

In addition to the on/off regulator, the controller network contains a current sensor and fault-logic circuitry. The fault logic permits manual control of the reservoir heater via the controller ON/OFF command in the event the regulator's output power transistor fails.

4.6.2 Command System

The command circuitry provides for the execution of the 8 discrete functions listed in Table 4-3. Each command is designed to accept inputs from either of two redundant spacecraft decoders. The Experiment ON/OFF command circuitry is totally redundant to prevent a single point failure resulting in loss of telemetry and therefore loss of the experiment. The Experiment ON/OFF circuitry also includes holding relays to permit independent operation of the ATFE, which shares a

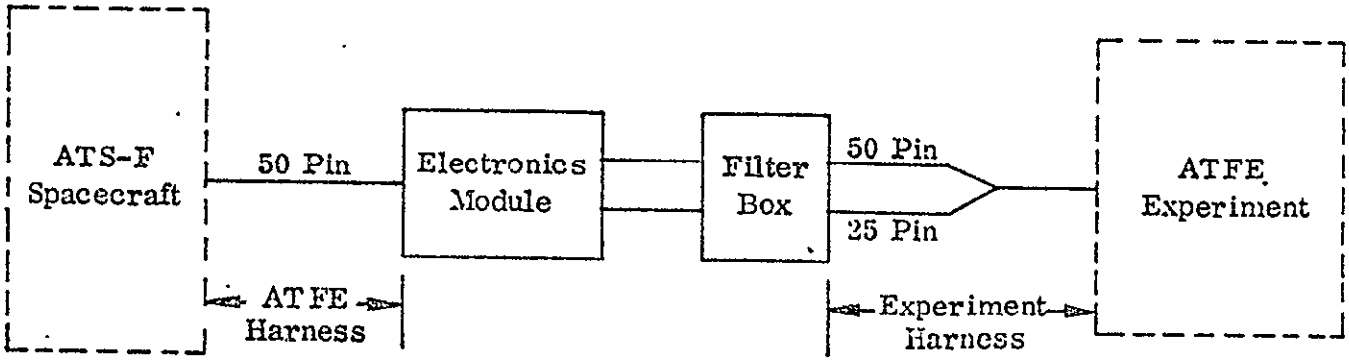

Fig. 4-5. Electrical interface

28-vdc load interface circuit (LIC) with the Quartz Crystal Microbalance Experiment. Loss of power from the LIC will cause a dropout to an Experiment OFF condition. Power can then be applied from the LIC only by exercising the Experiment ON command.

The backup and auxilliary heaters are included to ensure that failure of either the controller or the thermal diode will not result in an inability to demonstrate feedback control in space. The auxiliary heater is attached to the PCM box alongside the diode condenser saddle. It provides 20 W at 28-vdc and will be activated periodically if the thermal diode fails to transport the absorbed solar energy. This heater will also be used in conjunction with the thermal diode during the shadow period to further exercise the FCHP. The backup heater is identical to the reservoir heater that is regulated by the controller. It will be used to provide manual control of the FCHP if the controller should fail.

4.6.3 Signal Conditioning Unit

The ATFE signal conditioning unit operates from the 28-vdc ATFE bus and is activated by issuing the Experiment ON command. There are a total of 22 analog data outputs that are monitored through 11 channels on each of two redundant spacecraft encoders. The different telemetry channels are listed in Table 4-4. The data are derived from the controller current sensor and 20 separate temperature sensors. Except for the current sensor, the system is totally redundant in terms of sensors, signal conditioning, and output. Only the output is redundant for the current sensor.

Plantinum transducers are used to measure the absorber and radiator temperatures, which drop below that acceptable for thermistors. The remaining temperature data are sensed by single thermistors or thermistor composites. The transducer signal conditioning includes operational amplifiers, whereas the thermistor signal conditioning utilizes passive resistor divider networks.

4.7 Electromagnetic Interference (EMI) Shielding

The ATS-F is an advanced communications satellite whose antenna transmits at exceptionally high intensities over a broad frequency range. The ATFE is subjected to external electromagnetic radiation as high as 50 W/m over spot frequencies over the range from 40 MHz to 6 GHz. Preliminary tests indicated that the absorber and radiator telemetry channels were susceptible to EMI radiated both external and internal to the spacecraft. This susceptibility was experienced primarily at lower frequencies and manifested itself in unacceptable output voltage excursions that were apparently due to amplification of the EMI by the operational amplifiers in the signal conditioning circuits.

An aluminum box containing ferrite was installed as shown in Fig. 4-5 to filter EMI coming from the experiment harness. Three ferrite beads were also installed on each of the leads of the ATFE harness at the connector to filter EMI input from the spacecraft harness. The ATFE harness is wrapped with several layers of an electrically conductive cloth that is grounded to the connector and

the electronic module to shield the ATFE harness from the internal EMI involvement of the spacecraft. The experiment harness is similarly wrapped. The entire inboard side of the radiator was covered with three layers to reduce the EMI to the sensors while shielding was grounded with conductive epoxy to the ATFE chassis. This combination of shielding and filters has reduced the EMI susceptibility of the telemetry to within acceptable tolerances.

4.8 Support Structure and Thermal Insulation

4.8.1 Support Structure

The support structure consists of an aluminum sheet metal housing riveted to a lexan frame. In addition to providing the main support for the PCM box, the housing also includes brackets and a baseplate for attaching the electronics module and filter box. The lexan frame supports the absorber and radiator panels and provides the mechanical interface with the spacecraft. Aside from being a lightweight material with good strength, lexan has low thermal conductivity that minimizes the thermal interaction between the ATFE and the spacecraft. Lightening holes were machined into the frame, which decreased its weight and thermal conductance by approximately 70%.

4.8.2 Thermal Insulation

An insulation blanket is installed around the outside of the support structure to minimize the radiative coupling between the ATFE and the inside of the spacecraft. The blanket consists of alternate layers of singly aluminized mylar and nylon mesh enclosed

within singly aluminized kapton sheets. Similar insulation blankets are also installed within the ATFE (as indicated in Table 4-5) to minimize component interactions.

4.8.3 Component Integration

Various aspects of the mechanical integration of the different components have been indicated in the preceding sections. Essentially all mechanical interfaces are bolted to permit maintainability of the individual components. A low outgassing conductive grease was applied at all heat-pipe interfaces to reduce temperature drops through the system.

The condenser saddle of the diode is bolted to the PCM box which is, in turn, bolted to the FCHP evaporator saddle. Once instrumented and wrapped with insulation, this assembly is installed in the support structure and bolted to it at the flanges extending from the PCM box. Lexan washers are used at this interface to reduce conductive thermal losses from the PCM box. The individual radiator panels are then bolted to the FCHP and the lexan frame, as is the absorber panel. The main insulation blanket covers the support structure and is fastened to anchor nuts riveted to the structure. Finally, the electronics module and filter box are placed outside the insulation on the support structure standoff to which they are bolted. The instrumentation harness plugs into the filter box via two connectors and establishes the electronics interface between the experiment and the electronics module.

TABLE 4-4. ATFE TELEMETRY CHANNEL LIST

	Channel	Range, °C
1[a]	Absorber, near diode	-125 to +40
2	Absorber, near diode	
1	Diode adiabatic section	0 to +130
2	Diode adiabatic section	
1	PCM box, diode side	0 to +50
2	PCM box, diode side	
1	PCM box, FCHP side	0 to +50
2	FCHP saddle, upstream end	
1	FCHP, adiabatic section	-70 to +30
2	FCHP, adiabatic section	
1	Radiator, fin 1	-150 to +30
2	Radiator, fin 2	
1	Radiator, fin 5	-150 to +30
2	Radiator, fin 5	
1	Radiator, fin 10	-150 to +30
2	Radiator, fin 8	
1	FCHP gas reservoir	-75 to +30
2	FCHP gas reservoir	
1	Electronics module	-50 to +50
2	Electronics module	
1	Reservoir-heater current	0 to 200
2	(incl. fault-logic bias)	mA

[a] 1 denotes spacecraft encoder #1, 2 denotes spacecraft encoder #2.

TABLE 4-5. INTERNAL INSULATION BLANKETS

Description	Total number of layers
Absorber well	30
Absorber (inboard side)	39
Diode low-"k" section	13
Diode reservoir	13
PCM end plates	23
PCM box, including attached parts of diode and FCHP	19
FCHP transport section	5
FCHP feed tube	5
FCHP reservoir	11
Radiator (inboard side)	39

TABLE 5-1. QUALIFICATION AND ACCEPTANCE TEST

Test	Environment
Electromagnetic interference	Simulated RF
Functional	Ambient
Thermal vacuum	
Hot soak	51°C (qual.)/45°C (accept.)
Controller calibration	Nominal orbit
Baseline orbital cycle	Nominal orbit
Cold soak	-10°C (qual.)/-5°C (accept.)
Leak	Vacuum
Vibration	Sine and random
Leak	Vacuum
Functional	Ambient
Storage temperature	60° to -30°C (qual. only)
Instrumentation calibration	-90° to +50°C
Thermal vacuum	
Automatic feedback	Max., nominal, min. orbit
Manual feedback	Nominal orbit
Passive gas control	Nominal orbit
Automatic with auxiliary heater	Nominal orbit

TABLE 5-2. ACCEPTANCE THERMAL VACUUM TESTS

Solar cycle	Operational modes	Solar intensity	Spacecraft temperature, °C
1	Feedback control	Nominal[a] +5%[b]	20
2	Feedback control	Nominal +5%	35
3	Feedback control	Nominal -(5+8)%[c]	5
4	Feedback control	Nominal -5%	20
5	Passive gas control	Nominal -5%	20
6	Feedback control and auxiliary heater	Nominal -5%	20

[a] Nominal = 1350 W/m².

[b] ±5% = variation and uncertainty in the solar constant.

[c] -8% = seasonal variation due to change in the angle of incidence.

4.8.4 Spacecraft Interface

The ATFE is fastened to the east wall of the ATS-F in several locations through a 0.50 in. (1.27 cm) wide lexan flange extending around the frame. Teflon inserts are provided within the spacecraft wall to minimize the conductance at the bolted joints. The lexan frame minimizes the conductive interaction with the spacecraft skin, and the main insulation blanket reduces the radiative coupling between the ATFE and the inside of the spacecraft. The outside of the electronics module is black anodized so that it is radiatively coupled to the inside of the spacecraft in order to avoid the fluctuating thermal environment experienced by the ATFE absorber and radiator. The electronic interface is established by mating the experiment connector to the spacecraft connector. This contains all power, command, and telemetry functions.

5.0 GROUND TEST PROGRAM

5.1 Qualification and Acceptance

The ATFE was qualified and accepted for flight in accordance with the ATS-F Environmental Test Specification for Components and Experiments (S-320-ATS-2). The tests performed are summarized in Table 5-1 and are briefly described below.

To test for EMI susceptibility, the ATFE was mounted, in its flight configuration, to a simulated spacecraft east wall and irradiated with RF energy of the appropriate frequency and intensity

from both the exterior and interior of the spacecraft. The functional tests were performed in the ambient and therefore verified only the correct operation of the ATE, rather than providing quantative performance data. In determining the structural integrity of the diode, PCM box, and FCHP, the ATFE was placed in a vacuum chamber and a mass spectrometer and a helium leak detector were used to detect ammonia working fluid, octadecane PCM, and helium control gas from the diode, PCM box, and FCHP, respectively. The ATFE was subjected to both sine and random vibration in all three spacecraft axes. Storage temperature tests and instrumentation calibration were performed in an isothermal temperature-altitude chamber back-filled with dry nitrogen gas at near ambient pressure. Hot and cold soak tests were performed in a thermal vacuum chamber with liquid-nitrogen-cooled walls. After exposure to each of the environments described above, either the functional performance or the thermal performance during simulated orbital conditions was determined. Except for a slight shift in the controller set point on the flight unit, no degradation of the ATFE from environmental exposure was detected.

5.2 Thermal Vacuum Tests

The performance of the ATFE under simulated orbital conditions for various operational modes was of major interest and therefore comprised a significant portion of the testing program. The ATFE was mounted in a panel representing the east wall of the spacecraft. This panel formed one side of a box that radiatively simulated the internal

cavity of the spacecraft. The temperature of this box was then controlled to the desired spacecraft temperature. Foil heaters bonded to the inboard sides of the absorber and radiator were used to simulate absorbed solar energy. Voltage to the heaters was automatically stepped at 20-min intervals to the correct level corresponding to the solar energy cycle. Through the entire orbit, the absorber and radiator viewed the cold chamber walls. In addition to the flight instrumentation, 63 thermocouples were attached to various locations within the ATFE and the test setup to provide additional temperature data during qualification tests. Fifty thermocouples were used during the acceptance tests. All data were automatically logged at regular intervals with a commercial data-logging system.

The simulated orbital conditions for the various operational modes are listed in Table 5-2 for the acceptance thermal vacuum tests. The performance of the ATFE during the ground tests is compared to flight test results in a later section (6.3).

6.0 FLIGHT PERFORMANCE

The ATFE was tested extensively over the first three years since being launched into orbit on May 30, 1974. Each of the test modes identified in Table 3-1 has been exercised. Major emphasis has been on normal and passive mode operation. The data presented herein are derived from ten analog telemetry channels which measure temperatures

at different positions throughout the ATFE. An additional analog channel measures electric current to determine the status of the FCHP controller/reservoir heater.

Many of the results presented in this report are derived from previous reports on ATFE (Refs. 10 - 15). Information obtained from these reports has been modified and updated as required to best reflect the current understanding of the ATFE's performance.

6.1 Normal Mode Performance

The operation of the ATFE in the normal mode is described in detail in Section 3.0. The characteristic transient orbital performance of the experiment is presented in Fig. 6-1 for the normal mode 10 days after launch.

As the ATFE moves from the end of the shadow period into sunlight, the absorber (T-001) rapidly rises from -60°C to a maximum of 36°C near maximum solar input. As the sun "goes down" the temperature of the absorber drops below the PCM melt temperature (28°C) and diode reversal is initiated. Once diode shutdown is completed, the absorber cools rapidly and its temperature approaches its minimum steady-state condition asymptotically.

The PCM box (T-003) also increases rapidly in temperature once the diode begins transferring energy. It then reaches a plateau as the octadecane begins to melt. A gradient of approximately 3°C develops across the PCM box as the octadecane melt front advances from the diode

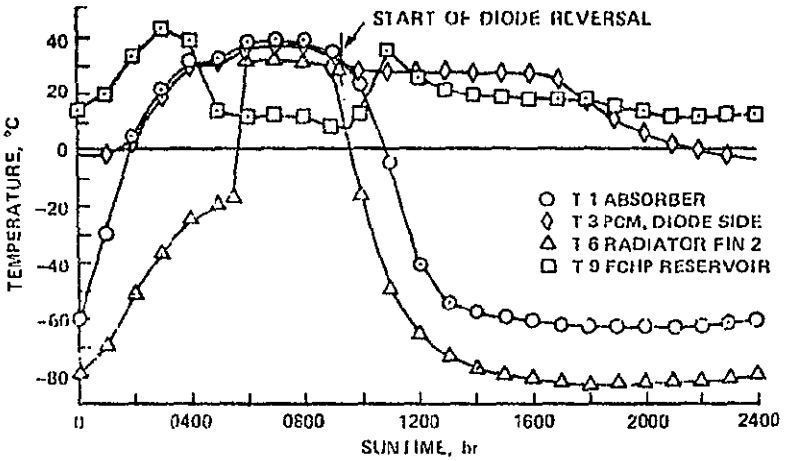

Fig. 6-1. Typical transient response in normal mode (10 days post-launch)

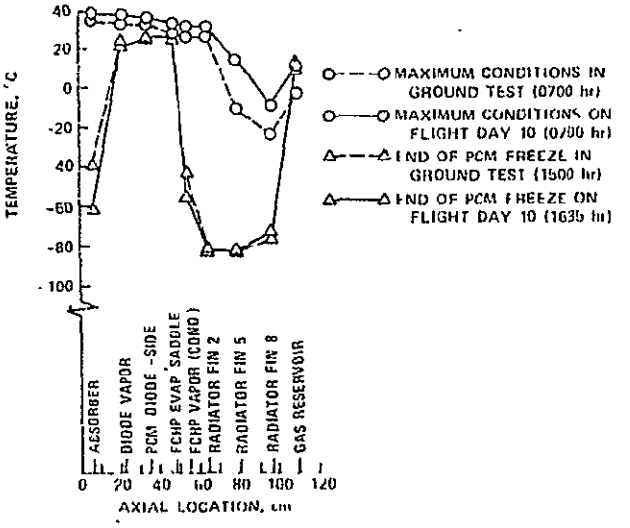

Fig. 6-2. Axial temperature profiles, flight day 10

.to the FCHP side of the box. The further increase in temperature from 31°C to 35°C is an overshoot resulting from inadequate cooling by the FCHP. This result relates to the performance of the FCHP reservoir (T-009), which at launch was 10°C warmer than the nominal design value and the temperature experienced during acceptance tests.

The higher reservoir temperature requires a higher vapor temperature for the FCHP to "open" and conduct heat. The resulting increase in vapor temperature is reflected directly in an increase in the temperature of the PCM box. A discussion of the potential cause of the elevated reservoir temperature is presented in a later section.

Beyond 0700 sun time the thermal energy transferred by the diode begins to decrease and the PCM temperature starts to drop. As the solar input decreases further, the absorber temperature drops below the PCM temperature and there is no longer any heat input from the diode (0945). The PCM continues to cool until it reaches 27.7°C at which time freezing begins. The latent heat released by the octadecane's freezing compensates for any transient losses during the diode and FCHP shutdowns. Further freezing compensates for the conductive losses through the diode and FCHP and any other parasitic losses from the PCM box. When all of the octadecane has frozen, the PCM box cools consistent with its parasitic heat leaks and its heat capacitance to just below 0°C before the start of the next daily cycle.

The solar input to the FCHP reservoir radiator during the initial portions of the cycle supplements the heat power applied to the reservoir by the controller and results in a rapid increase in reservoir temperature (T-009). When the temperature of the diode side of the PCM box (controller sensor location) reaches the set point (29°C), the reservoir heater turns off and the reservoir temperature begins to decrease. As the reservoir temperature decreases the control gas in the FCHP recedes into the reservoir. This unblocks the FCHP condenser section and permits the heat pipe to transport energy from the PCM to the radiator fins. Once all of the PCM has melted, the FCHP begins to transfer the energy to the radiator (T-006), where it is dissipated to space.

When the diode-side PCM temperature drops below 29°C the controller turns the reservoir heater back on with a resulting increase in reservoir temperature. This causes the FCHP to shut down and results in a corresponding cooling of the radiator. Continued cooling of the radiator and subsequent cooling of the reservoir result from diminishing solar input as the shadow period is approached.

The ATFE's thermal performance is further illustrated by the axial temperature distributions shown in Fig. 6-2. At the time of maximum energy throughput (0700) there are slight temperature drops across the absorber/diode, the PCM box, and the active portion of the FCHP. Radiator fins 5 through 10 which are located at the inactive portion of the FCHP exhibit thermal gradients consistent with the conduction losses from the active portion and the gas reservoir. For this cycle,

the reservoir heater has been off since 0400, and at 0700 the reservoir has reached a quasi-steady-state temperature of 11.5°C. At maximum conditions, the radiative coupling from the hot absorber inhibits cooling of the reservoir, and causes its temperature to be higher than the effective sink temperature (e.g., fin 8).

During the shadow period, the PCM box is essentially isothermal and large gradients develop betewen the PCM and the absorber and radiator as the diode and FCHP shut down. In the normal mode, conditions are such that the PCM has completely frozen by 1630. At this time the PCM is at 27°C, and the absorber and radiator have reached equilibrium temperatures of -62 and -82°C, respectively. The 6°C gradient between the PCM and the diode transport section (T-002) indicates that the diode is fully shut off, with liquid blockage extending through the "low-k" and at least part of the transport section (Ref. 2). The -55°C temperature in the FCHP transport (T-005), and the 82°C gradient between it and the PCM is indicative of gas blockage back into the FCHP evaporator.

Throughout the entire shadow period, the reservoir heater is on continuously and the reservoir temperature achieves an equilibirum value of 14°C, which is sufficient to maintain complete shut-off of the FCHP. At the end of the shadow, the PCM box is still isothermal but has dropped to 0°C. The absorber and radiator temperatures show a slight increase that is due apparently to infrared inputs from the spacecraft antenna, which are at a maximum at the beginning and end of shadow.

6.2 Feedback Versus Passive Control

The operation of an electrical feedback-controlled heat pipe is in principle the same as that of a passive "cold-reservoir" variable conductance heat pipe (VCHP). The only difference is that the FCHP's reservoir temperature is regulated to provide the desired control. In the passive system the reservoir follows the sink temperature and the heat-pipe vapor and heat-source temperatures adjust accordingly. The normal and passive modes provide a comparison of the ATFE's performance with the two types of control. In addition, operation at an elevated set point can be effected by using the auxiliary and back-up heaters. This test gives a direct comparison of the temperature stability afforded by a gas-controlled VCHP with and without feedback.

6.2.1 Normal Versus Passive Mode Performance

In Fig. 6-3 the ATFE's transient performance in the normal mode is compared with its performance in the passive mode. The diode's performance (i.e., T-001) is not included since its transient behavior is the same in both modes. In the passive mode the controller is turned OFF and the feedback pipe operates as a conventional "cold-reservoir" system. Hence, during the period of solar input, the reservoir has a sinusoidal temperature profile which increases from -75°C to a maximum of 10°C and then cools back to -75°C and holds through the shadow. At approximately 0400 the VCHP begins to open and transport energy to the radiator. This is evidenced by the sharp

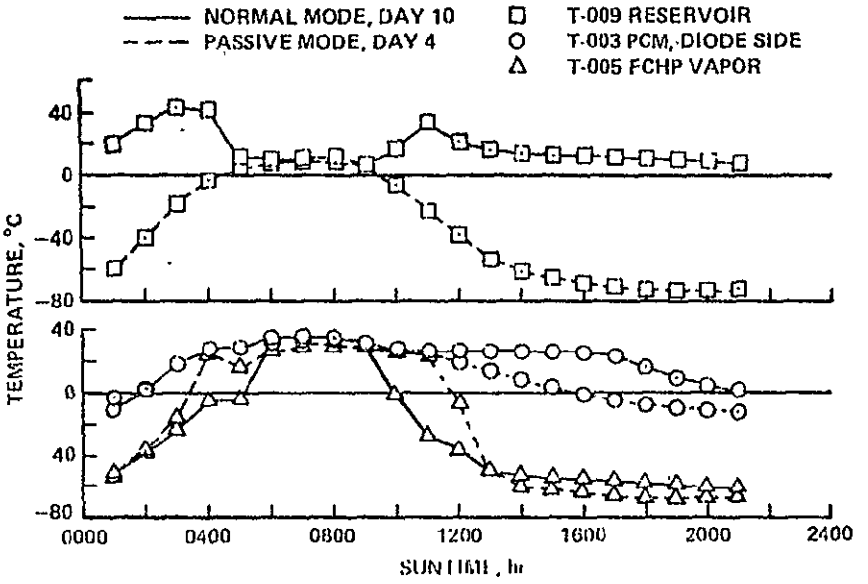

Fig. 6-3. Comparison of feedback and passive transient control

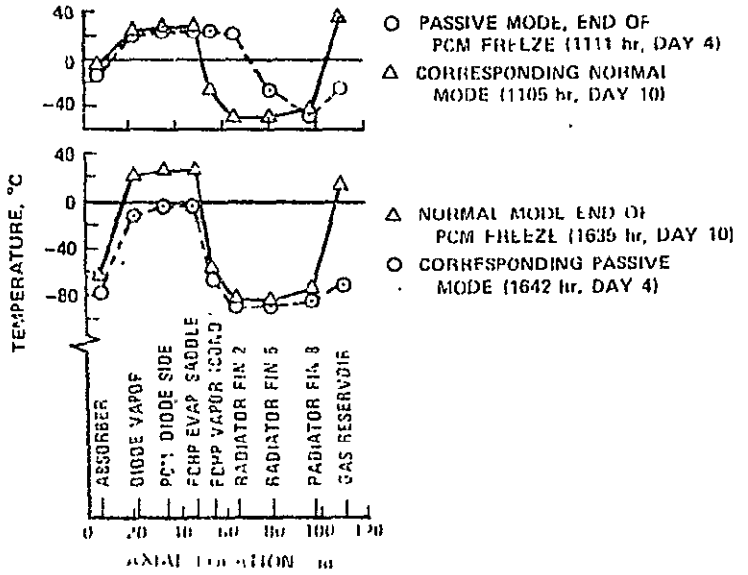

Fig. 6-4. Comparison of axial profiles in normal and passive modes

rise in the pipe's transport temperature (T-005). The more rapid increase in the temperature of the reservoir compared to the heat pipe causes a partial shutdown of the VCHP at 0500. As the maximum condition is approached the conditions are such that the VCHP opens up again and remains open through 1100 in the passive mode. Freezing of the PCM occurs between 1000 and 1100 as the open VCHP transfers the PCM's latent heat. Subsequent cooling by the VCHP reduces the PCM and pipe temperature to the point where, even though the reservoir is very cold, the heat pipe shuts down. This is indicated by the sharp decrease in T-005.

The major difference in the performance of these two modes of operation is due to the passive VCHP's being open when the PCM starts to freeze. As a result, all the stored latent heat is transmitted to the radiator. In the normal mode, where feedback is employed, the reservoir is heated when T-003 drops below 29°C. This causes the FCHP to shut down prior to freezing, and it remains shut off until the next day's solar input brings the PCM to above 29°C. Consequently, temperature stability is provided for six to seven hours in the normal mode, versus one hour with passive control.

Axial temperature profiles for these modes are compared in Fig. 6-4 at the end of each of their respective freezing periods. The end of freezing occurs at 1111 in the passive mode. The heat-piping action during this time is evidenced by the isothermal region of the VCHP which extends through the second radiator fin. At the same time,

In the cycle with feedback control the FCHP is shut off back to the downstream end of the evaporator. Freezing is completed at 1635 in the normal mode, and the pipe is still completely shut off. The passive mode profile at this time also shows the VCHP shut off, but this is because the PCM's latent energy had been dissipated more than 5 hours earlier and its temperature has dropped below 0°C.

6.2.2 Feedback Control at an Elevated Set Point

The operation of the FCHP in the normal mode just discussed is essentially that of an "ON-OFF thermal switch." The ATFE was designed to demonstrate regulated FCHP energy dissipation during solar input at a nominal 29°C set point (measured at the PCM). However, because the in-flight reservoir temperatures exceed the maximum reservoir design temperature of 5°C, an overshoot of PCM temperature occurs and regulated control at 29°C is not possible.

A demonstration of the FCHP's ability to provide temperature regulation was obtained by running the system at an elevated set point. This was accomplished by operating in the backup/auxiliary mode. In these tests, the control temperature was pre-set to 46°C and the backup reservoir heater was then manually commanded ON or OFF consistent with the prevailing PCM temperature (T-003). As in the case of automatic control, the backup heater is ON when T-003 is below the set point and the FCHP shuts down. Conversely, the heater is OFF when T-003 is above the set point.

The auxiliary heater is used in this test to provide thermal throughput during the shadow and the early and late portions of the solar cycle when the thermal diode is OFF. This heater has a 20-W output and is attached to the diode side of the PCM box. Basically it replaces or supplements the thermal energy transferred by the diode during its forward-mode, heat-pipe operation.

A comparison of the temperature stability provided with feedback versus passive control during the elevated set point tests is presented in Fig. 6-5. The results show that with feedback, the PCM temperature is controlled at 46 ± 2°C throughout the entire cycle. Tests were conducted through only a portion of the shadow since quasi-steady operation is obtained then. Passive control, under the same conditions, results in a peak PCM temperature of 45°C and a steady-state shadow condition with the PCM box at 25°C.

The major control provided by the FCHP during these tests lies in its regulation of the heat dissipation throughout a very broad variation in sink temperature. Radiator fin #10, which is in the inactive region of the heat pipe is a good measure of the effective sink temperature. It varies from -56° during the shadow to a maximum of 26°C. The feedback system therefore provides control to within ±2°C corresponding to an 82°C variation in sink temperature.

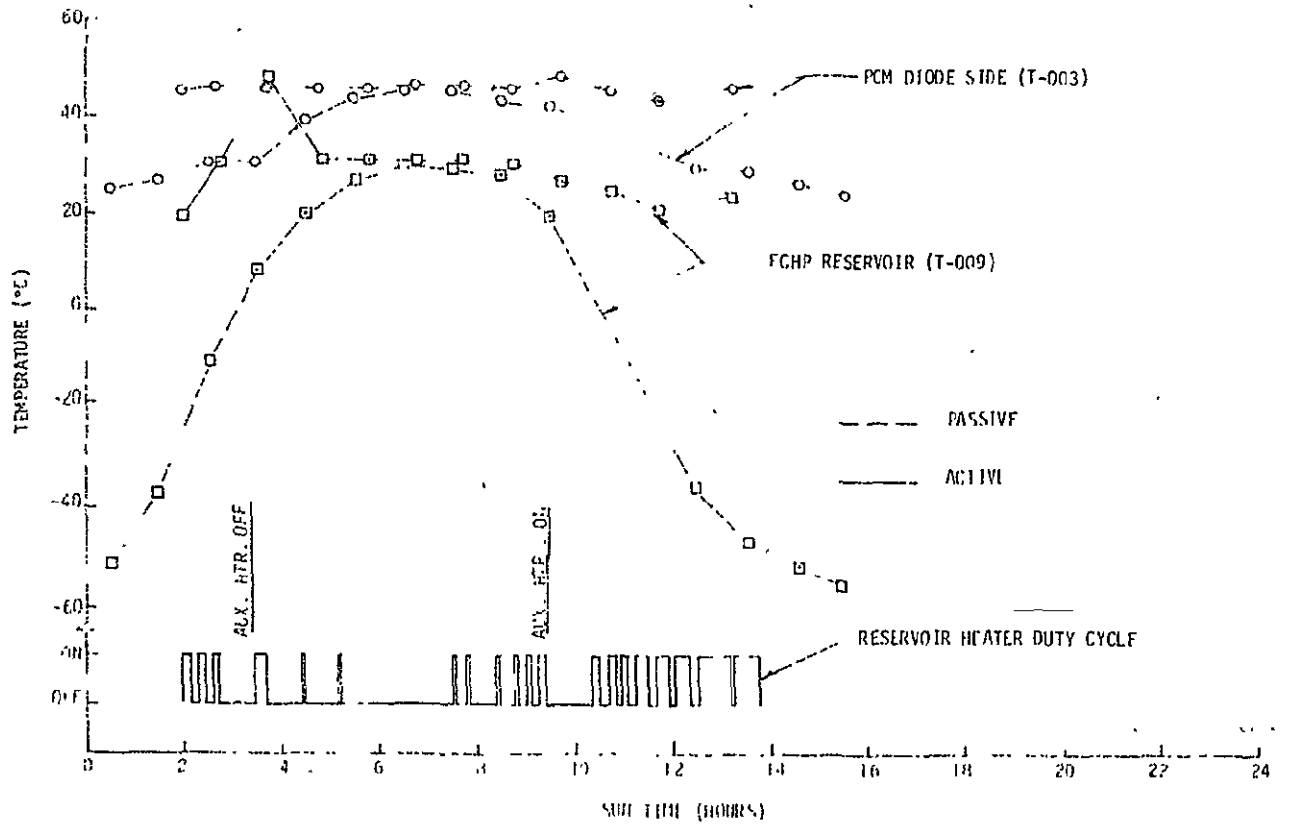

Fig. 6-5. Comparison of feedback and passive control at an elevated set point

6.3 Comparison of Flight and 1-g Performance

Flight data for the normal mode on day 10 is compared with data obtained with the pre-flight thermal vacuum acceptance tests in Figs. 6-6 and 6-7. Solar input during the ground tests was simulated by electrical heaters attached to the inboard side of the absorber, radiator, and FCHP reservoir surfaces. The input for this ground test was based on a solar intensity of 395 Btu/hr-ft^2, whereas the actual solar intensity on flight day 10 was 381 Btu/hr-ft^2. An absorptivity of 0.96 was used for the absorber's black paint. The radiator and reservoir are covered with second-surface mirrors, for which a nominal design absorptivity of 0.10 was used to establish the heater input.

The transient response of the ATFE presented in Fig. 6-6 is similar in the flight and ground tests. There are some discrepancies worth noting, however. As can be seen in both Figs. 6-6 and 6-7, the flight temperatures during the hours of peak solar insolation (peak @ ~ 0700) are higher at all locations. The most noticeable increase occurs at the FCHP gas reservoir (T-009) which is running approximately 15°C warmer on flight day 10. The hotter reservoir causes the entire FCHP to operate at a higher temperature (see Section 4.4) and this, in turn, causes the PCM (T-003) to run warmer. Thus, the efficiency of the entire absorber-to-radiator heat transfer path is impaired by the higher reservoir temperature. It has been determined that the higher reservoir temperature is due to degradation of the second-surface mirrors which act as the reservoir's radiating surface. This is discussed in Section 6.4.2.

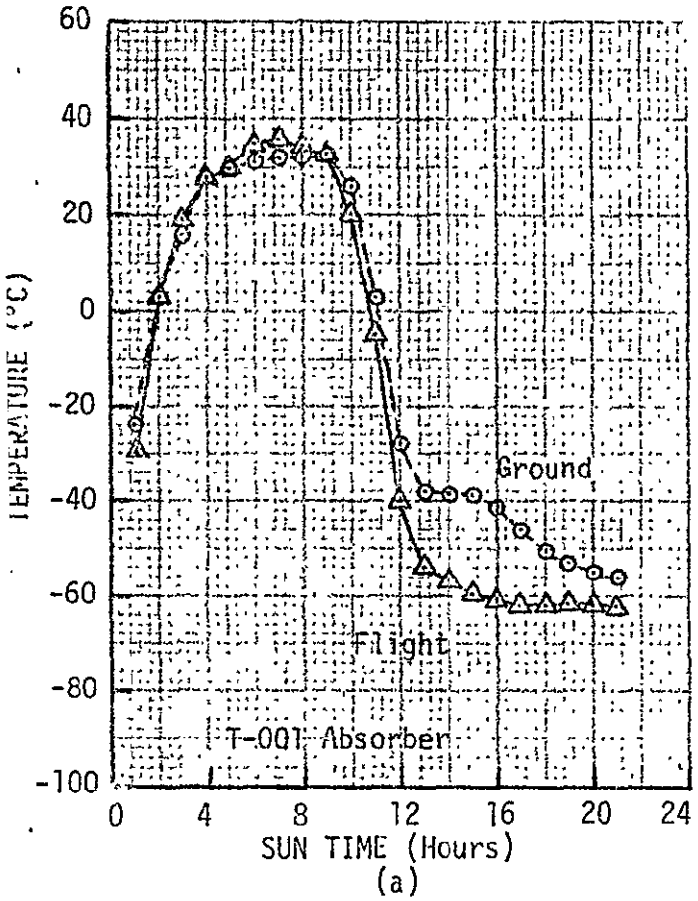

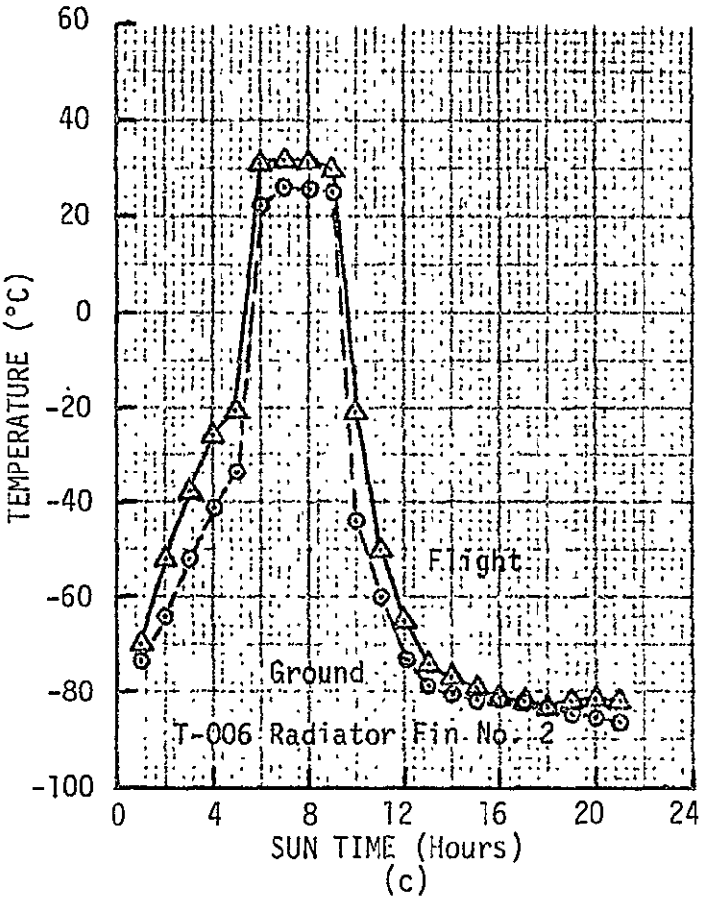

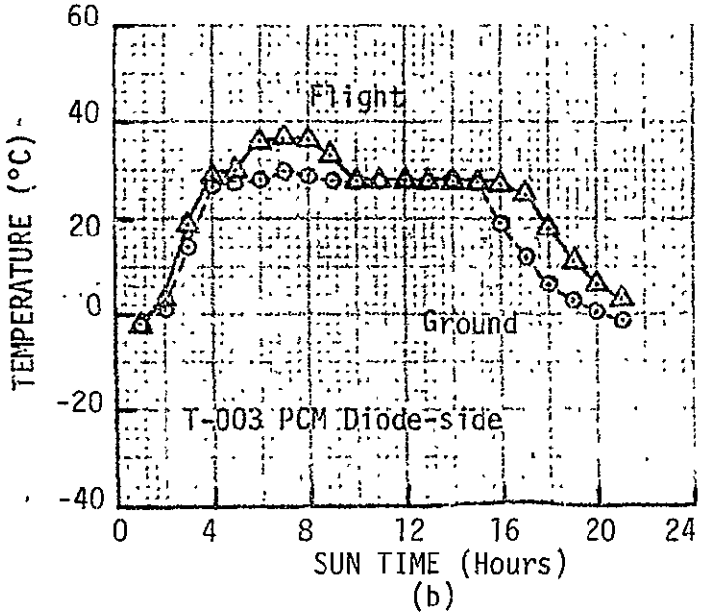

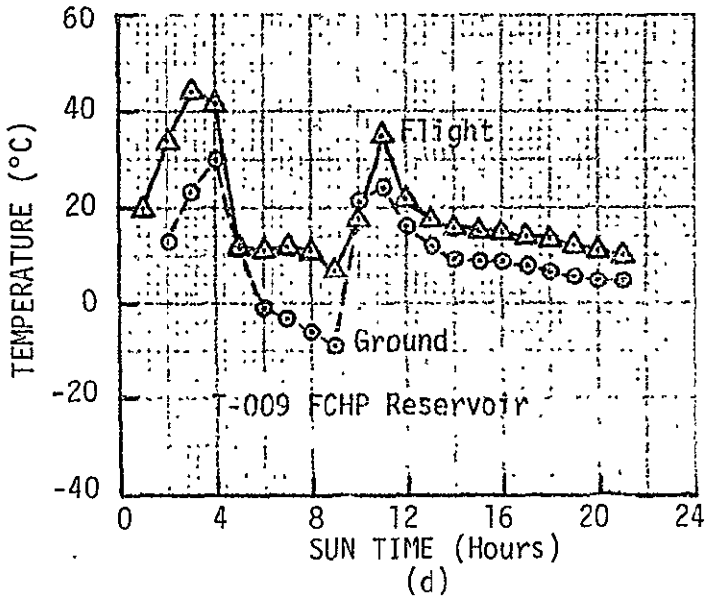

Fig. 6-6. Comparison of flight and ground transient performance - normal mode

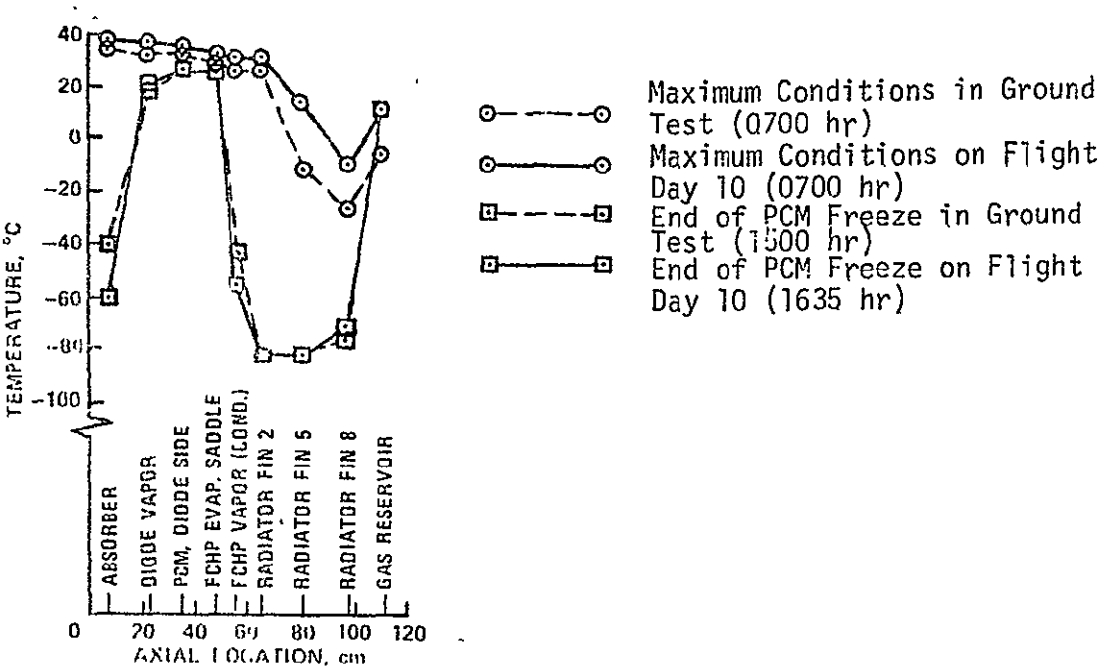

Fig. 6-7. Comparison of flight and ground axial temperature profiles

Another difference in thermal performance between the flight and ground tests is indicated by lower absorber temperatures (T-001) on flight day 10 during the shadow period (see Fig. 6-6a). This lower temperature implies that the diode is conducting less heat between the PCM and the absorber subsequent to diode shutdown. This is further supported by the fact that the time required for complete freezing of the PCM increased from 5.5 hours during ground tests to 6.5 on flight day 10 (see Fig. 6-6b). A lower diode OFF conductance would decrease the parasitic losses from the PCM and increase its freeze interval. This is discussed in more detail in Section 6.4.4.

The behavior of the PCM was the same in both ground and flight tests. The melting and freezing points were both approximately 28°C and the gradient across the box, less than 3°C during peak solar conditions, indicates that the thermal conductance is unaffected by the 0-g environment.

6.4 Long Term Performance

6.4.1 Telemetry

Certain anomalies were encountered while reducing the flight data for the ATFE and it was suspected that some of the telemetry data was unstable. An analysis was performed to determine the validity of this data (see Ref. 15 for details). By comparing the long term trends of all the channels and by examining quai-steady-state results derived from auziliary mode tests, it was deduced that the channels on the radiator (T-006, -007, -008) and absorber (T-001) were indeed drifting.

These channels have very sensitive signal conditioning networks. This was necessary to accommodate the low temperature (~ 190°K) and broad range that they monitored. Low resistance platinum transducers which require amplification of their output signals are used for these channels. All other channels (T-002, -003, -004, -005 and -009) use thermistors and resistance divider circuits which are much more stable.

A shift in the calibrations which caused radings that were higher than normal was observed during the flight acceptance tests. At that time resistors were replaced in the circuits which provides a constant current source to the transducers. It is possible that the telemetry shift in flight is also due to a drift in this constant current cource. This drift could be caused by the fact that the electronics module has been running as high as 40°C during maximum conditions, while the components are typically rated at 20°C.

The analysis reported in Ref. 15 was performed after a year and a half of flight time. Since that time, it appears that these channels have stabilized and are no longer drifting. Adjustments have been made in all subsequent analyses to account for these shifts.

One further problem with the telemetry data is that some of the channels became saturated at maximum conditions. Specifically, channels T-006, -007 and -008 in DACU 2 do not read any higher than 37°C, 16°C and 26°C, respectively. However, sufficient data exists and this does not impair the analytical efforts.

6.4.2 Degradation of Second-Surface Mirrors

As noted previously, the temperature of the ATFE during the hours of peak solar insolation was higher immediately following launch than in the ground tests and it has been increasing with time. The probable cause of this is a degradation of the second-surface mirrors (optical solar reflectors -OSR) that are employed as radiator surfaces for the FCHP's condenser and reservoir.

Selected flight data for the first two and one half years of orbit are presented in Fig. 6-8a. The data show the maximum daily temperature (@ ~ 0700 hr. sun time) for the PCM (T-003) and the FCHP reservoir (T-009) versus days in orbit. The reservoir temperature near the end of the PCM freeze period (~/600 hr.) is also shown in this Fig. At both locations the maximum daily temperature is increasing with time: T-003 increased from 36°C at launch to 54°C on flight day 949, while T-009 increased from 11°C to 47°C over the same interval.

The FCHP reservoir temperature (T-009) during the shadow period in the normal mode remains constant at about 16°C. This supports the earlier conclusion (Section 6.4.1) that this channel is stable and that the trends noted during the maximum solar conditions are caused by something other than telemetry drift.

The seasonal variation of solar intensity incident on ATFE is shown in Fig. 6-8c. The variations of both incident solar angle and solar irradiance were used in calculating the intensity. If Figs.

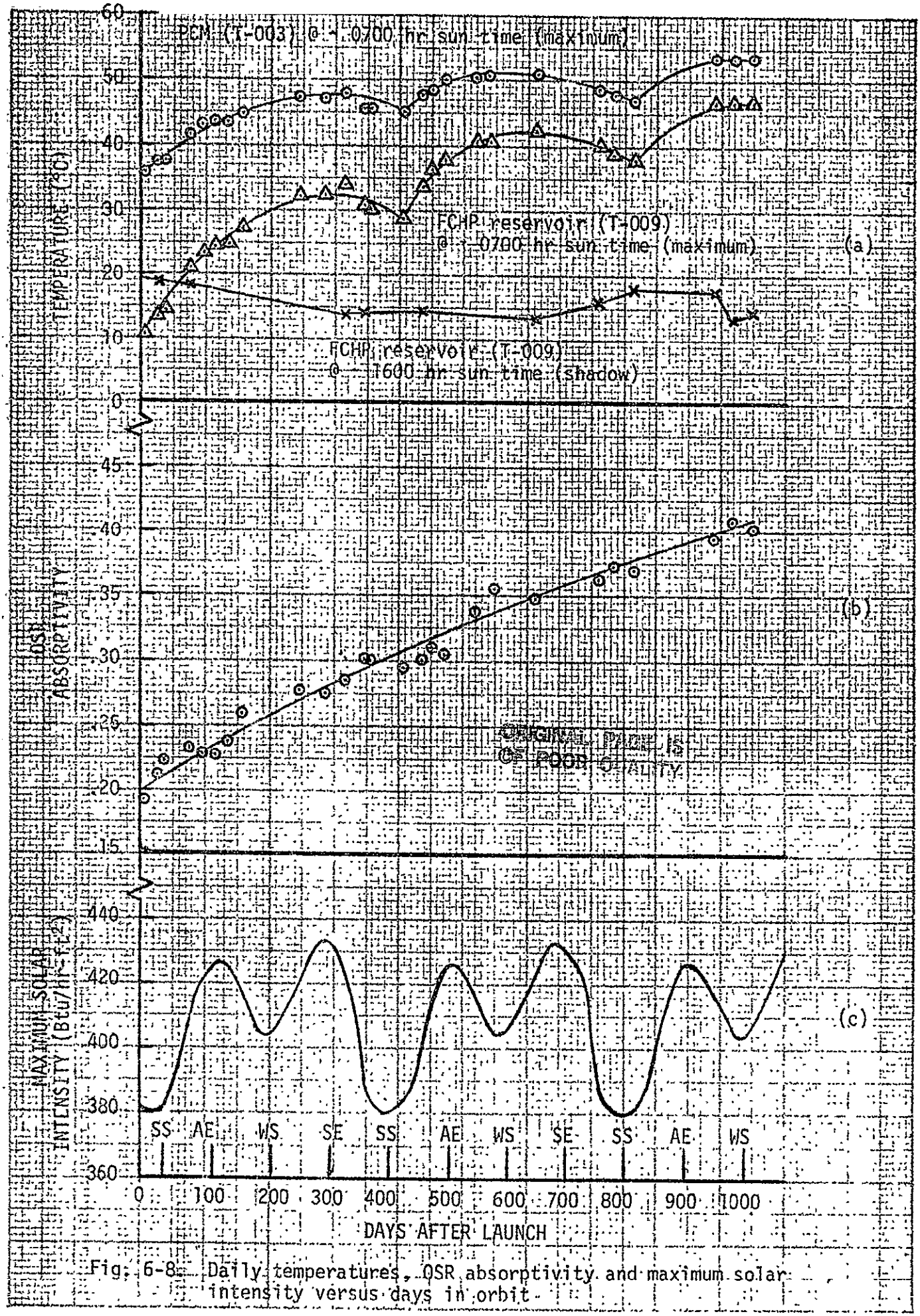

Fig. 6-8 Daily temperatures, OSR absorptivity and maximum solar intensity versus days in orbit

6-8a and 6-8c are examined concurrently it can be observed that the rates of increase of the maximum temperatures for both T-003 and T-009 are greatest during the period of increasing solar intensity prior to the spring and autumn equinoxes (designated as SE and AE). The temperatures tend to decrease slightly prior to the summer and winter solstice (SS and WS).

During maximum conditions the PCM is completely melted and the absorbed heat is transported from the PCM box to the radiator via the FCHP. The higher the gas reservoir temperature during this time, the more difficult it is for the FCHP to open; i.e. to increase its thermal conductance. The operating temperature of the FCHP has increased 1°C for every 2°C increment in reservoir temperature in order to continue transporting the heat input. The increase in FCHP temperature is reflected directly in the temperature of the PCM box.

The outboard face of the reservoir is in the plane of the radiator and views deep space continuously. Its surface, like the radiator's, is covered with OSR's to permit maximum cooling with solar input. Design values used for the mirror's optical properties were $\alpha/E = 0.10/0.82$.

A thermal analysis of the reservoir was conducted to determine the cause of the elevated temperatures (see Ref. 11 for details). The heat balance included solar and infrared inputs, radiation to space, and parasitic radiative and conductive heat flows. Flight data were used in the analysis. The OSR absorptivity which satisfied

the thermal balance at each selected data point was calculated. The results of this analysis are plotted in Fig. 6-8b.

The effective absorptivity of the OSR's has increased from approximately 0.19 at launch to 0.41 two and one half years later. The oscillation of the individual data points around the mean is due to the sinusoidal variation of the maximum solar intensity. The high points occur at the solstices, when the intensity is lowest (see Fig. 6-8b and 6-8c). This is due to the inverse relationship between α and the solar input which occurs in the equation defining the reservoir heat balance. This equation slightly over-compensates for seasonal effects, thus causing the variance from the mean.

The conclusion that the measured ATFE temperatures are due to a degradation of the OSR's was further supported by flight simulation tests conducted with the ATFE Flight Back-Up Unit at NASA/ARC. During these tests electrical inputs were applied to the radiator system, including the FCHP gas reservoir, to simulate a solar input corresponding to an $\alpha = 0.20$ (Ref. 12). This was the effective absorptivity calculated for an early flight day. The temperature profiles exhibited by the AFTE during this test were in much closer agreement with the early flight temperature profile than those exhibited during the Flight Acceptance tests, during which an $\alpha = 0.10$ was used to determine heater input.

There is no well defined reason for the high degradation rates experienced by the ATFE's OSR panels. It is possible that the mirrors are cracking due to discharge of the silver coating. This phenomenon apparently occurs because of a difference in electric potential between the mirror and the substrate to which it is bonded.

In any case, a larger reservoir on the FCHP would have provided a greater design margin. The added mass would result in slightly slower response, but overall it would represent a design improvement.

6.4.3 Phase Change Material Box (PCM)

The function of the phase change material package was to provide the ATFE with temperature stability. It accomplishes this by absorbing or rejecting heat nearly isothermally as the fusible material melts and freezes in the course of its orbital cycle. The fusible material chosen for the ATFE was octadecane because its melting temperature (28°C) is within the desired operating range and because it has a high heat of fusion and a stable melting point.

Flight data indicate that the PCM performed as predicted through more than 1800 melt/freeze cycles in a 0-g environment. The PCM melting point was stable at 27.9°C. The normal mode melting interval was 1.3 hr. when the PCM was subjected to a thermal throughput of approximately 20 W. This is consistent with the 26 W-hr of latent heat energy that the 384 gm charge of octadecane was predicted to supply.

The PCM freezing point remained stable at 27.4°C. The normal mode freezing interval was consistently 6.4 hours. In the passive mode, without the benefit of FCHP shutdown to prevent the heat from escaping through the radiator, PCM freeze occurred in 1.3 hours. The subcooling averaged 0.5°C and was less than 0.7°C in all cases.

6.4.4 Thermal Diode Heat Pipe

The thermal diode heat pipe has effectively performed its major design functions during its exposure to the 0-g environment. Every day it has transported an average of 20 W of solar input between the absorber and PCM during its forward mode of operation. Then when the absorber temperature drops below the PCM temperature during the daily shadow period, it shuts down, minimizing the reverse flow of energy. This behavior is illustrated in Figs. 6-1 and 6-2 which show the axial temperature profiles and transient response at the beginning of flight. While the absorber stabilizes at about -60°C throughout the shadow period the PCM drops only slightly below 0°C at the end of the shadow period. This is directly due to low OFF conductance of both the diode and the FCHP which isolate the PCM from heat sinks at the absorber and radiator.

The diode's behavior, nevertheless, does indicate some apparent degradation. Fig. 6-9 shows the temperature gradients between the diode vapor temperature and the PCM for sun and shadow conditions in the passive and normal modes as a function of time. During the maximum solar input (~ 0700 sun time) the temperature drop is increasing

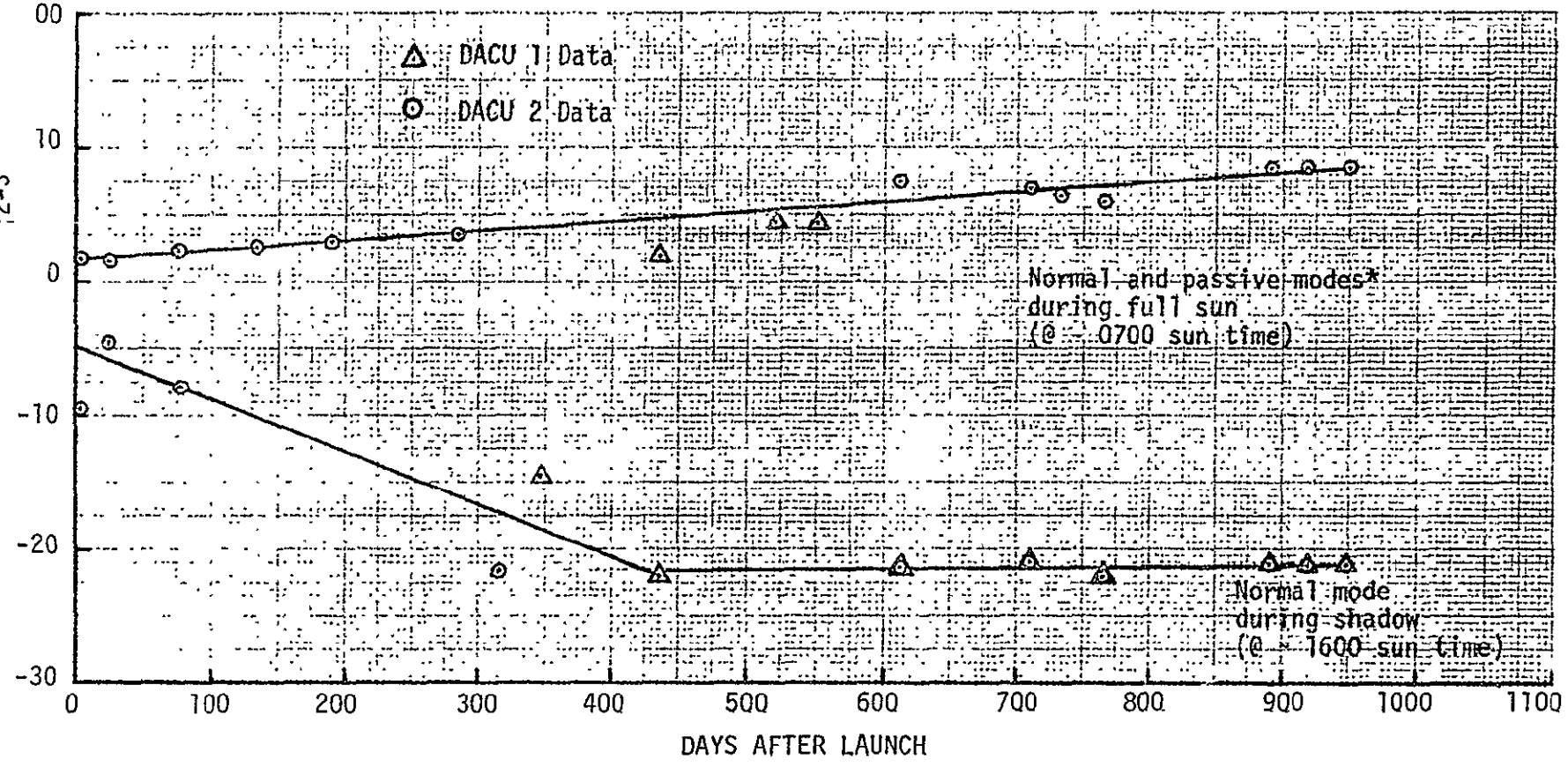

*Normal and passive mode are the same during full sun since FCHP reservoir heater is OFF

Fig. 6-9. Diode PCM temperature drop versus days in orbit

steadily at a rate of .007 °C/day. However, in the shadow period the temperature drop increases initially and then levels off after approximately one year.

These two trends indicate that non-condensible gas blockage is occurring. In the shadow period the shutdown blockage has advanced from the transition/low k mitre joint (see Fig. 4-1) to somewhere in the forward mode condenser. The temperature drop remains constant after the gas front reaches the condenser section because at this point all two phase transfer beyond the condenser is inhibited. The amount of axial heat conduction is independent of the degree of gas blockage and remains constant; thus, the temperature drop (ΔT_{2-3}) in the shadow stabilizes as indicated in Fig. 6-9.

However, during the forward mode of operation (@ ~ 0700 sun time) the temperature gradient continually increases. This is because the effective conductance decreases proportionally with the increased gas blockage and decreased effective condenser length. Hence forward mode performance is degrading slightly.

6.4.5 Feedback Controlled Heat Pipe (FCHP)

The FCHP has experienced a steady increase in its operating temperature throughout the flight tests. As noted previously, this is due to the degradation of the second surface mirrors which cover the reservoir's radiator. This has led to a higher reservoir temperature which causes the entire heat pipe to run warmer. However, the heat pipe itself has not degraded while in orbit. It has transported as

much as 30 W in the forward mode, it has performed effectively as an OFF/ON thermal switch to minimize temperature fluctuations at the PCM control point and, at an elevated set point, it was capable of providing temperature stability with variations in heat load and effective sink temperature.

6.5 End of Mission

During the last two to three years of its mission, the ATFE was operated primarily in the passive mode. It was without electrical power and the acqusition of telemetry data was suspended. However, the ATFE was still subjected to a daily solar cycle with all components responding in the passive mode.

A final set of telemetry data was obtained in early July, 1979, after more than five years in orbit. The ATFE was operated in both the normal and passive modes during the data acquisition period. The data indicate that the ATFE is functioning much the same as it was during the first two and one half years. The trends observed with respect to the OSR degradation and the diode's non-condensible gas generation are elaborated below.

The peak temperatures after 1859 days in orbit had increased to 58°C and 53°C at the PCM (T-003) and gas reservoir (T-009), respectively, compared to 53°C and 47°C on day 949 (see Fig. 6-8). This indicates that while the temperatures are still increasing due to the degradation of the second surface mirrors, the rate of increase has slowed. The

effective absorptivity of the OSR's has degraded to 0.47 on day 1859 from 0.41 on day 949.

The five year data also indicate that the non-condensible gas generation in the diode has stopped. The temperature gradient between the diode's vapor and the PCM is essentially the same as it was after two and one half years (see Fig. 6-9). Finally the behavior of the PCM was virtually unchanged from ground tests through five years of daily freeze/thaw cycles in space.

7.0 REFERENCES

1. Swerdling, B. and Kosson, R., "Design, Fabrication and Testing of a Thermal Diode," NASA CR-114526, Nov. 1972.

2. Swerdling, B., et al., "Development of a Thermal Diode Heat Pipe for the Advanced Thermal Control Flight Experiment (ATFE)," AIAA Paper 72-260, 1972 (also in AIAA Progress in Astronautics and Aeronautics: Thermal Control and Radiation, Vol. 31).

3. Bentilla, E. W., et al., "Research and Development Study on Thermal Control by Use of Fusible Materials," Northrop Space Laboratories, NASA N66-26691, April 1966.

4. Hale, D. V., et al., "Phase Change Material Handbook," NASA CR-73475, Sept. 1970.

5. Bienert, W., Brennan, P. J., and Kirkpatrick, J. P., "Feedback Controlled Variable Conductance Heat Pipes," AIAA Paper 71-421, 1971 (also in AIAA Progress in Astronautics and Aeronautics: Fundamentals of Spacecraft Thermal Design, Vol. 29).

6. Anon, "Study to Evaluate the Feasibility of a Feedback Controlled Variable Conductance Heat Pipe," Tech. Summary Rept., NASA CR-73475, Sept. 1970.

7. Depew, C. A., et al., "Construction and Testing of a Gas-Loaded Passive-Control Variable Conductance Heat Pipe," NASA CR-114597, June 1973.

8. Marcus, B. D., "Theory and Design of Variable Conductance Heat Pipes," NASA CR-2018, April 1972.

9. Bienert, W. and Brennan, P. J., "Transient Performance of Electrical Feedback Controlled Variable Conductance Heat Pipes," ASME Paper 71-Av-27, July 1971.

10. Kirkpatrick, J. P. and Brennan, P. J., "The Advanced Thermal Control Flight Experiment," AIAA Paper 73-757, 1973.

11. Suelau, H. J. and Brennan, P. J., "Advanced Thermal Control Flight Experiment Thermal Analysis - First Progress Report," prepared for NASA/ARC under P. O. 8380 B(KT), December 1974.

12. Suelau, H. J. and Brennan, P. J., "Advanced Thermal Control Flight Experiment Thermal Analysis - Second Progress Report," prepared for NASA/ARC under P. O. 8380 B(KT), March 1975.

13. Kirkpatrick, J. P. and Brennan, P. J., "Performance Analysis of the Advanced Thermal Control Flight Experiment," AIAA Paper 75-727, May 1975.

14. Kirkpatrick J. P. and Brennan, P. J., "ATS-6: Flight Performance of the Advanced Thermal Control Flight Experiment," IEEE Transactions on Aerospace and Electronic Systems, Vol. AES-11, No. 6, November 1975.

15. Brennan, P. J., "Summary Report for Thermal Analysis of ATFE Flight Data," prepared for NASA/ARC under P. O. A 15055 B(KT), December 1975.